1-1-2005

Structure, detrital zircon U-Pb ages and 40Ar/39Ar geochronology of the Early palaeozoic Girilambone Group, central New South Wales: subduction, contraction and extension associated with the Benambran Orogeny

Christopher L. Fergusson
University of Wollongong, cferguss@uow.edu.au

C M Fanning
Australian National University

D. Phillips
University of Melbourne

Benjamin Ackerman
University of Wollongong

Structure, detrital zircon U-Pb ages and 40Ar/39Ar geochronology of the Early palaeozoic Girilambone Group, central New South Wales: subduction, contraction and extension associated with the Benambran Orogeny

Abstract

The Early Palaeozoic Cape River Metamorphics consist mainly of psammitic gneiss and schist and occur as an extensive linear belt at the western margin of the Charters Towers Province 200 km southwest of Townsville in the northern Tasmanides. A prominent foliation (S_2) is the main structure in the belt and is associated with tight to isoclinal folds, subparallel mineral and intersection lineations, and boudinaged pods of vein quartz and pegmatite. In the southwest, the main foliation is a crenulation cleavage (S_2) related to D_2 deformation. It overprints steeply dipping foliation (S_1) formed in a D_1 deformation but no associated folds have been found. Gently plunging, upright, open folds (D_3 deformation) with axial planar S_3 crenulation cleavage have affected the main foliation (S_2). These deformations were associated with upper greenschist to lower amphibolite facies metamorphism. Amphibolite-grade orthogneiss containing S_2 and S_3, deformed granite and migmatite of the Fat Hen Creek Complex occurs in the northeast. In the southwest, the main foliation (S_2) is folded around a map-scale, gently plunging synclinorium indicating that S_2 formed with a subhorizontal orientation. In metamorphic rocks, the origin of widespread, intense subhorizontal foliation, usually associated with recumbent folds, has been considered problematic and in many cases is attributed to crustal extension. We relate the origin of D_2 structures to subvertical shortening (i.e. extension) resulting in orientations that are strikingly divergent to those of upright D_1 and D_3 structures that were induced by compression. The proposed extensional event is poorly constrained in timing but it affected much of the Fat Hen Creek Complex, the oldest known phase of which is 493 Ma, and occurred prior to $^{40}Ar/^{39}Ar$ cooling ages at 423 – 409 Ma that also post-dated the D_3 deformation.

Keywords

Structure, detrital, zircon, ages, 40Ar, 39Ar, geochronology, Early, palaeozoic, Girilambone, Group, central, South, Wales, subduction, contraction, extension, associated, Benambran, Orogeny, GeoQUEST

Disciplines

Life Sciences | Physical Sciences and Mathematics | Social and Behavioral Sciences

Publication Details

Fergusson, C. L., Fanning, C., Phillips, D. & Ackerman, B. (2005). Structure, detrital zircon U-Pb ages and 40Ar/39Ar geochronology of the Early palaeozoic Girilambone Group, central New South Wales: subduction, contraction and extension associated with the Benambran Orogeny. Australian Journal of Earth Sciences, 52 (1), 137-159.

Structure, detrital zircon U-Pb ages and $^{40}Ar/^{39}Ar$ geochronology of the Early Palaeozoic Girilambone Group, central New South Wales: subduction, contraction and extension associated with the Benambran Orogeny

C. L. FERGUSSON[1*], C. M. FANNING[2], D. PHILLIPS[3] AND B. R. ACKERMAN[1]

[1]*School of Earth and Environmental Sciences, University of Wollongong, NSW 2522, Australia.*
[2]*Research School of Earth Sciences, The Australian National University, ACT 0200, Australia.*
[3]*School of Earth Sciences, University of Melbourne, Vic. 3010, Australia.*

Running Title: Girilambone Group of central New South Wales

The Girilambone Zone is located in the northern part of the central subprovince of the Lachlan Fold Belt and its bedrock exposure includes the widespread Girilambone Group. This unit consists of two main components, low-grade, metamorphosed quartz-rich turbidites and bedded chert with Middle to Late Ordovician conodont ages in the west (Ballast Formation), and low to moderate-grade schist, psammitic schist, mafic schist and phyllite that occur in the east. Detrital zircon grains from samples of a quartzite and a quartzose psammite from the eastern part of the Girilambone Group around Girilambone, have age spectra (500–600 Ma) typical of Ordovician turbidite successions in southeastern Australia. In the Girilambone district, an intense, steeply dipping differentiated layering (S_2) formed in the D_2 deformation and has largely masked the effects of earlier deformation apart from foliation (S_1). S_2 is overprinted by mainly north-trending, moderately to steeply west-dipping crenulation cleavage (S_3) that is axial planar to abundant open to close folds (D_3 deformation). Locally, S_3 cleavage and fold axial planes have a low dip. In the Tottenham district, the main foliation is also a differentiated layering (S_2) with low to moderate dips to the southeast in a northern domain and subhorizontal in a larger southern domain due to folding by abundant near-isoclinal, recumbent folds (F_3). These reflect ductile thinning of the crust and are attributed to extensional deformation. Weak to locally intense crenulation cleavage and associated folds (D_4) affect the S_2 in the northern domain and are weakly developed in the southern domain. Three muscovite $^{40}Ar/^{39}Ar$ ages from both the Girilambone and Tottenham regions are *ca* 435 Ma consistent with deformation and metamorphism during the Late Ordovician – Early Silurian Benambran Orogeny. The Girilambone Group in the Late Ordovician was accreted in an inferred subduction complex related to an east-dipping subduction zone in the Wagga marginal sea. The subduction complex in the Early Silurian was affected by contractional and extensional deformation prior to the migration of igneous activity from the Molong island arc to the Wagga-Omeo Zone.

KEY WORDS: $^{40}Ar/^{39}Ar$ ages, Benambran Orogeny, Girilambone Group, structure, U-Pb zircon ages.

[*]Corresponding author: cferguss@uow.edu.au

INTRODUCTION

Deformed and variably metamorphosed Ordovician quartz-rich turbidite successions are widespread in the Lachlan Fold Belt of southeastern Australia (VandenBerg & Stewart 1992). The Girilambone Group underlies much of northern central New South Wales and has been shown to consist, at least in part, of Ordovician rocks with an inferred deep-water turbidite association (Felton 1978; Stewart & Glen 1986; Iwata et al. 1995). Nevertheless, some uncertainty remains that either an older basement unit of probable Cambrian age is included within the Girilambone Group or the unit consists of deformed and variably metamorphosed Ordovician turbidite rocks (Scheibner & Basden 1998, p. 133). This paper reports the results of structural mapping and geochronological studies (detrital zircon age spectra and $^{40}Ar/^{39}Ar$ ages) undertaken to address this issue in the Girilambone and Tottenham districts (Figure 1). We present an interpretation of the tectonic history of the Girilambone Group in the context of proposed subduction complexes within the Lachlan Fold Belt (Gray 1997; Gray & Foster 1997; Fergusson 2003) and also in terms of the significance of the Benambran Orogeny (Collins & Hobbs 2001).

BACKGROUND

The northern part of the central subprovince of the Lachlan Fold Belt consists of the Wagga-Omeo and Girilambone Zones (Figure 1b). The Wagga-Omeo Zone is dominated by low-grade to high-grade regionally metamorphosed Ordovician quartz turbidites intruded by abundant granitic rocks (Gray 1997). In contrast, the Girilambone Zone has considerably less granite and contains the widespread Girilambone Group, which consists of metasandstone, slate, phyllite, psammitic schist, pelitic schist, and quartzite with less abundant chert, mafic schist and serpentinite.

The western part of the Girilambone Group commonly has only one main cleavage, is of low metamorphic grade and contains sedimentary structures indicative of turbidite deposition (Iwata et al. 1995). Within these rocks Stewart and Glen (1986) and Iwata et al. (1995) have found late Middle to early Late Ordovician fossils in bedded chert. These rocks have been called the Ballast Formation but locally do include rocks of greater structural complexity and apparently higher metamorphic grade that is more typical of the eastern part of the Girilambone Group (Iwata et al. 1995). Iwata et al. (1995) also reported that equivalents of the uppermost Silurian to Lower Devonian Cobar Supergroup have been incorrectly mapped as part of the Girilambone Group. Fleming et al. (2001) suggested that as much as 50% of the area of the Girilambone Group is potentially part of the Cobar Supergroup.

The eastern part of the unit includes the Girilambone district where T. Hopwood, in a study reported by Smith (1971), found a complicated stratigraphic succession with multiple deformations and a complex regional map pattern. In more recent work, Fogarty (1996, 1998) used a two-fold subdivision with an older unit of basement schist containing numerous crenulation cleavages unconformably overlain by two units, the Caro Schist and Tritton Formation, consisting of less structurally complicated greywacke, shale, psammitic schist, quartzite, phyllite and mafic schist.

Around Tottenham (Figure 1), the Girilambone Group is called the Tottenham Subgroup and consists of biotite-bearing pelitic to psammitic schist (Bogan Schist) with two units of

mafic schist and quartz-magnetite rock (Mount Royal and Carolina Forest Formations) in addition to undifferentiated psammitic and pelitic schist (Sherwin 1996). Further to the south, 8 km west of Tullamore (Figure 1) low-grade rocks mapped as part of the Girilambone Group still preserve sedimentary structures (Sherwin 1996). North of Condobolin, Scott (2000) mapped another unit within the Girilambone Group, the Murda Formation that is distinguished from the remainder of the Girilambone Group by the presence of magnetite-bearing sandstone and also contains chert with long-ranging Late Ordovician conodonts.

Several ultramafic to mafic intrusive complexes occur in the Girilambone Group in the Tottenham and Condobolin districts (Figure 1). One of these, the Bulbodney Creek Intrusive Complex is located 10 km southwest of Tottenham and has no surface exposure (Sherwin 1996). Its circular shape is deduced from magnetics and it is considered to have intruded the Girilambone Group. U-Pb zircon ages of 1050 Ma, 1100 Ma and a younger age of 448 ± 4 Ma determined by SHRIMP have been quoted by Sherwin (1996) from the complex. The younger age has been regarded as an intrusive age whereas the older ages are considered inherited grains. The Murrumbogie Intrusive Complex occurs 20 km east-northeast of Condobolin and consists of mafic intrusive rocks with a U-Pb zircon SHRIMP age of 413 ± 5 Ma (unpublished age in OZCHRON, GA Sample ID 90844022, available from Geoscience Australia http://www.ga.gov.au/oracle/ozchron/TOC.jsp).

Much of the landscape underlain by the Girilambone Group is either covered by a thin veneer of alluvial sediments or is very weakly dissected with sparse bedrock exposure. Where outcrop does occur, it is low lying and usually weathered. The most plentiful and informative exposures occur in road and railway cuttings and in open-cut mines. Airborne geophysical surveys have been flown for the Geological Survey of New South Wales in the Narromine-Nyngan and Cobar-Nymagee 1:250 000 map sheets and provide some constraints on the regional structure (Kevron Geophysics Pty Ltd 1995a, b; Tesla Airborne Geoscience Pty Ltd 1999a, b).

GIRILAMBONE DISTRICT

Rock types

In the Girilambone district, the Girilambone Group is dominated by a psammitic (quartzose metasandstone) lithology with pelitic layers (slate), less abundant quartzite, mafic schist and serpentinite (Figure 2). Relatively fresh exposures of psammite occur near an access road at 0477044 6543514 (Coolabah (8235) 1:100 000 sheet) and this contains dispersed grains of detrital quartz 0.5–1 mm across with undulose extinction, less common plagioclase in a matrix of quartz, muscovite and chlorite with grains less than 0.1 mm across (Figure 3a). The groundmass has dynamically recrystallised quartz grains and aligned muscovite flakes defining a foliation. Accessory tourmaline and zircon are present. Most lithic clasts are no longer discernible due to recrystallisation but must have included a range of quartz-rich and some micaeous types. In general, psammitic rocks in the open-cut pits at Girilambone Copper Mine and along the disused Nyngan-Bourke railway have a laminated appearance due to a differentiated layering (see below). These rocks are texturally similar to the psammite described above with relict detrital grains, including detrital muscovite, and dynamically recrystallised grains in the matrix.

Relict bedding is visible in many exposures with alternating psammitic and pelitic layers (e.g. Hartmans and Murrawombie Pits, railway cuttings 14.5 km northwest of Girilambone).

Pelitic layers consist mainly of muscovite with less abundant quartz and chlorite with no apparent detrital mica. Pelitic layers are usually no more than 5–10 cm thick and are less abundant than psammite although pelitic intervals in the unit may well be recessive and poorly represented in the available exposure. Sedimentary structures are well preserved at one long rail cutting 14.5 km northwest of Girilambone and include graded beds, loadcasts (Figure 3b), various Bouma layers including Bouma C micro-crosslaminated layers (Figure 3c). Graded bedding also occurs below the lower bench in the northern part of Hartmans Pit (Figure 4). These features indicate the turbidite origin of the original succession and are consistent with observations to the west at Yanda Creek (Felton 1978) and to the southeast near Tullamore (Figure 1; Sherwin 1996).

Quartzite forms low ridges and smaller outcrops in the district and is also associated with ore deposits (Fogarty 1996, 1998). Texturally, they are similar to the psammites with minor relict detrital quartz grains in a matrix dominated by quartz and less common muscovite. The matrix and the margins of detrital quartz grains are dynamically recrystallised. We agree with Shields (1996) that these rocks were originally quartz-rich sediments and not chemical sediments.

Mafic schist occurs in the Murrawombie Pit (Figure 5) and is widely associated with copper mineralisation in the Girilambone district (Fogarty 1996). At least some of these rocks are deformed intrusions within the succession and are possibly related to other mafic and ultramafic intrusions in the region (Fogarty 1998). One sample from the Tritton prospect has relict plagioclase grains typically 1 mm across with all the primary mafic minerals altered to an assemblage of chlorite, epidote, calcite, albite and quartz. It contains one main foliation defined by seams of aligned chlorite and concentrations of opaque minerals. A sliver of serpentinite occurs along a fault in Murrawombie Pit and has been traced to the northwest (Fogarty 1996).

Given the uniformity of most rocks in the available exposure we have been unable to map any lithological subdivisions in the Girilambone district apart from recognising that some units of quartzite and mineralization are mappable for distances of hundreds of metres and locally further. We have been unable to discern any regional variations in the geophysical images (magnetics and radiometrics) compiled for the Geological Survey of New South Wales (Kevron Geophysics Pty Ltd 1995a, b; Tesla Airborne Geoscience Pty Ltd 1999a, b) consistent with subdivisions within the Girilambone Group and this contrasts markedly with the obvious magnetic banding in the Cobar Supergroup to the west.

Structure

The structure of the Girilambone Group in the Girilambone district is dominated by a strong foliation reoriented by folds with axial planar crenulation cleavage(s). The main foliation is laminar in appearance and is a differentiated layering with quartz-rich and micaeous domains mainly up to 5 mm across (Figure 6a). Considerable variation occurs in the orientation of the differentiated layering and crenulation cleavages that formed after it, which compounds difficulties for attempting correlations between distant outcrops. On the basis of available overprinting criteria we have inferred four deformation phases.

Evidence for D_1 deformation is only recognised microscopically and is manifest as early cleavage (S_1) defined by aligned muscovite and elongate quartz grains in the microlithons of the main S_2 differentiated layering (Figure 6a). Little can therefore be deduced about D_1 in the

Girilambone district apart from it having formed a continuous cleavage. Bedding trends are east-southeast to east-west and dips north (Figure 7a).

D_2 deformation produced the widely developed differentiated layering (S_2). Metamorphism synchronous with D_2 is indicated by the strong foliation with aligned muscovite and quartz along with dynamic recrystallisation of the rocks (Figure 6a). In the northern part of the Girilambone district, S_2 is mainly steeply dipping and strikes easterly to southeasterly (Figure 7b). In many outcrops S_2 is subparallel or at a low-angle to bedding which is consistent with tight to near isoclinal folds being produced by D_2. The L_2 intersection lineation is rarely found and has a range in plunge from steep to gentle to the northwest (Figure 7c). Sub-biotite grade greenschist facies metamorphism has only accompanied the first two ductile deformations.

The main structure associated with the D_3 deformation is a moderately to steeply west-dipping crenulation cleavage (S_3) that is well developed in the northern open-cut pits of the Girilambone Copper Mine (Figure 6b) and in the exposures along the disused Nyngan-Bourke railway to the northwest of Girilambone (Figure 7d). The crenulation cleavage consists of microlithons up to 2–3 cm across with cleavage planes defined by concentrations of muscovite and opaque minerals having formed by dissolution. S_3 is axial planar to abundant open to close folds in S_2 with characteristic low amplitude-to-wavelength ratios that are typical of folds associated with crenulation cleavages (Gray 1979). Intersection lineations (L_3) and fold hinges (F_3), in general, plunge gently to the north but many hinges in Murrawombie Pit have westerly plunges (Figures 5, 7e). In Hartmans Pit, enveloping surfaces associated with these folds are steeply inclined to the north as shown by relict bedding preserved in the western side of the pit (Figure 4). In Murrawombie Pit, structures associated with the D_3 deformation are more complex with less well-developed axial planar crenulation cleavage and zones with abundant polyclinal folds. Where developed, the axial planar crenulation cleavage (S_3) shows significant changes in orientation with local gentle to moderate dips to the north (Figures 2, 5). In outcrops 12 km to the southeast of Girilambone, along the disused Nyngan-Bourke railway line, the main crenulation cleavage is gently dipping to the west and northeast similar to some orientations of S_3 in Murrawombie Pit (Figure 2). It is possible that in these areas, two crenulation cleavages and associated folds formed during two distinct deformation phases but the lack of overprinting criteria and exposures do not allow them to be distinguished.

The D_4 deformation is represented by weak crenulation cleavages and associated open to broad folds that are locally present and overprint S_2 and more rarely S_3. Cleavage planes have formed by dissolution with no new mica growth. Two main orientations are recognised, (1) S_{4A}, an east-southeast trending steeply dipping crenulation cleavage with folds plunging gently to the north, and (2) S_{4B}, a gently dipping to subhorizontal crenulation cleavage with an intersection lineation plunging gently to the north (Figure 7f-i). These two sets of structures have not been observed at the one location and therefore no overprinting criteria have been found between them.

Additionally in the open-cut pits of Girilambone Copper Mine late brittle faults are exposed in the high-walls and postdate all the ductile structures. They are mainly moderately dipping north-striking faults with typically only small displacements (metres or less) where they can be determined.

TOTTENHAM DISTRICT

Rock types and lithostratigraphy

Exposures with relatively unweathered rocks occur in road and railway cuttings between Tottenham and Tullamore on and adjacent to the weakly dissected bedrock ridge that forms the drainage divide between the Bogan River and Bulbodney Creek. In contrast to the bedrock around Girilambone, the Tottenham district contains biotite-bearing regional metamorphic rocks with schist in the north and phyllite in the south (Figure 8). The northern part includes the Tottenham Subgroup with three schist units and some undifferentiated Girilambone Group rocks (Sherwin 1996). Due to the intensity of deformation, stratigraphic relationships cannot be established between the schist units mapped by Sherwin (1996). The trends of these units are subparallel to the strike of the main foliation. It is not possible to establish stratigraphic relationships as bedding is only rarely preserved and orientation is based on the main foliation in the rocks (see below). No indicators of stratigraphic way up have been identified. Individual mafic schist units either are part of the same unit repeated by folding or are different units as implied by the stratigraphic terminology of Sherwin (1996).

Around Tottenham exposure is scarce apart from road and rail cuttings and the distribution of these units was partly indicated by the distribution of copper mine shafts, which occur in the mafic schist units (Suppel 1975; Sherwin 1996). The aeromagnetic image (Kevron Geophysics Pty Ltd 1995a) indicates that many narrow magnetic anomalies are present east of Tottenham (Figure 8). These magnetic anomalies are interpreted as lenses of mafic schist and quartz-magnetite rocks. Evidence for this is based on the occurrence of mafic schist in a low rail cutting at 0540367 6430240 (Kerriwah (8333-II & III) 1:50 000 sheet), which is located on one of these magnetic anomalies. The mafic schist has mineral assemblages that include epidote, chlorite, muscovite, calcite, plagioclase and quartz (Sherwin 1996). 15 km east-southeast of Tottenham is the Minemoorong Intrusive Complex (Figure 8); this is one of several ultramafic complexes in the region and has no surface exposure but a prominent ovoid magnetic anomaly (Sherwin, 1996).

Mica schists around Tottenham are medium to fine grained (0.5 to < 0.1 mm grain size) and contain quartz, muscovite, biotite and chlorite. Rare detrital muscovite and tourmaline is present. Biotite is only found in the schist in the immediate vicinity of Tottenham and has not been found further to the southeast beyond Albert (Figure 8). Most of the schist contains abundant quartz veins and pods of vein quartz. Locally, more micaeous layers indicate relict bedding. The quartz-rich nature of much of the schist indicates that it was probably mainly derived from psammitic rocks. Most of the rock is statically and dynamically recrystallised in quartz-rich layers. Graphitic schist containing sparse fine-grained graphite occurs at a few localities (e.g. 0541974 6414982 Kerriwah (8333-II & III) 1:50 000 sheet) and Sherwin (1996) mapped several strongly foliated metachert units over distances in excess of 12 km in the Girilambone Group 25–50 km south of Albert.

South of Albert towards Tullamore the grainsize of the quartz-mica schist decreases and the rock type is predominantly a siliceous phyllite (Figure 9). Grainsize reduction between the schist and phyllite is gradual and therefore the contact is gradational; its approximate location is shown on Figure 8. The siliceous phyllite consists mainly of quartz with minor muscovite and was probably derived from quartzose psammite.

Structure

The Tottenham district is divided into two domains: a northern (I) and southern domain (II; Figure 8). In the northern domain the strike of the main foliation is subparallel to the

lithological boundaries of the mafic schist units and is also subparallel to relict pelitic and psammitic lithological layering. The main foliation is a differentiated layering (Figure 9) and has formed from the crenulation and differentiation of an earlier structure, and is therefore designated S_2. S_2 is defined by aligned biotite and muscovite at Tottenham indicating upper greenschist facies regional metamorphism (Yardley 1989) that accompanied deformation. At Tottenham, S_2 is moderately dipping to the southeast (Figure 10a).

East of Tottenham the foliation along with the trends of mafic schist units defines a steeply inclined, asymmetric antiform with a moderate plunge to the southeast (the "Orange Plains Anticline" of Sherwin 1996). Foliation in mafic schist is defined by compositional banding and crudely aligned chlorite. In rail and road cuttings 5–7 km east-southeast of Tottenham, a moderate to steep, east-dipping crenulation cleavage (S_{4A}) is developed on the steep eastern limb of the antiform (Figures 8, 10b). This structure is labelled S_{4A} rather than S_3 to maintain consistency with the structural succession of the southern domain because no S_3 has been mapped in the northern domain. S_{4A} is marked by the development of centimetre-width microlithons with well-developed muscovite aligned in cleavage domains. Some rocks contain relict ovoid porphyroblasts now replaced by aggregates of chlorite and muscovite (?cordierite, e.g. 0533545 6432545 and 0540367 6430240 Kerriwah (8333-II & III) 1:50 000 sheet). S_{4A} wraps around these the porphyroblasts implying that they developed prior to D_4 and possibly during D_2. Thus locally metamorphic conditions associated with D_2 may have been in the lower amphibolite facies but D_4 was associated with greenschist facies conditions.

S_{4A} is axial planar to tight to close, upright folds in S_2 and S_2 parallel quartz veins. These folds all verge to the west consistent with the location on the eastern limb of the map-scale F_4 antiform. An intersection lineation (L_{4A}) plunges moderately to the southeast (Figure 10c). In the southern part of domain I west of the Minemoorong Intrusive Complex, the crenulation cleavage (S_{4B}) and axial planes of associated folds dip steeply to the west-southwest in contrast to its orientation further north (Figures 8, 10b, d). S_{4A} and S_{4B} have slightly different orientations but have similar appearances and the same style of associated folds. They are assumed to reflect the same deformation as they are not observed in the same outcrops and do not interfere with each other.

In the southern domain the main foliation (S_2) is gently dipping to subhorizontal (Figure 10e). Foliation is defined by aligned muscovite and elongate, strongly recrystallised quartz. At one location (0551724 6402953 Tullamore (8432-I & IV) 1:50 000 sheet), pressure fringes developed adjacent to fine pyrite defines an east-west stretching lineation. Lithological layering is parallel to the foliation. The main structure is also a differentiated foliation derived from the crenulation of an earlier slaty-style cleavage and is therefore labelled S_2. No folds in the lithological layering with axial planar S_2 have been recognised, although the widespread occurrence of an east-west trending intersection lineation (L_2) indicates the plunge of F_2 folds (Figure 10f).

Throughout the southern domain the subhorizontal orientation of the main foliation reflects abundant, recumbent, tight to near isoclinal F_3 folds (Figure 9a). The folds are angular with planar limbs and have relatively high amplitude-to-wavelengths ratios. Fold hinges trend 100º and are slightly to moderately oblique to the L_2 intersection lineation (Figure 10f, g). The L_2 intersection lineation is folded around many of these F_3 hinges and therefore predates these folds (Figure 9b). In F_3 fold hinges, axial planar cleavage is poorly developed whereas on the fold limbs S_2 and S_3 are well developed and are either subparallel or at a very low angle to each other making their discrimination difficult. Late northwesterly to northerly trending folds (Figure 10h) are formed that postdate the F_3 folds and are similar in orientation to late structures of the northern domain but lack axial planar foliation. They account for locally

steeper dips in the dominantly gently dipping main foliation of the domain. Weak upright east-west trending late folds also locally affect the southern domain.

A cross section between Tottenham and Tullamore shows the relationship of biotite-bearing schists at Tottenham to the regional structure (Figure 11). These rocks record the highest metamorphic grade in the region but potentially higher and/or equivalent grade rocks occur 7 km east-southeast of Tottenham where altered porphyroblasts occur in muscovite-chlorite bearing schists. South of Albert, the schist changes to finer-grained phyllite containing a muscovite-chlorite-quartz assemblage, the decrease in grainsize could be reflection of grainsize reduction during recrystallisation that accompanied deformation and/or a decrease in metamorphic grade. Further south, 8 km west of Tullamore, rocks occur with well-developed sedimentary structures and no sign of the intense foliation of the siliceous phyllites further north (Sherwin 1996). These rocks are similar to those of the Ballast Formation in the western part of the Girilambone Group although the relationship between these rocks and the siliceous phyllite is not exposed.

In the northern domain (I) the main foliation dips moderately to the southeast whereas in the southern domain (II) the foliation is mainly subhorizontal (Figure 11). The implication is that the structurally lowest rocks with respect to S_2 and S_3 are the biotite-bearing rocks at Tottenham. However, it cannot be ruled out that intense retrogression accompanied by dynamic recrystallisation has destroyed biotite in schist and phyllite south of Tottenham.

GEOCHRONOLOGY

Detrital zircon ages

Two samples of psammite were collected for detrital zircon age analysis using the SHRIMP at the Australian National University. Sample TH1 is a quartzite from the prominent quartzite ridge west of Girilambone (0489975 6541257 Coolabah (8235) 1:100 000 sheet; Figure 2). Sample GG2 is from a bedrock exposure of quartzose psammite with weakly developed foliation (S_2) from adjacent to a road 20 km west of Girilambone (0477044 653514 Coolabah (8235) 1:100 000 sheet).

Sixty one and sixty zircon grains respectively were analysed following standard procedures for detrital zircon age analysis (Williams 1998). U/Pb ratios were calibrated relative to the standard FC1 from the 1099 Ma Duluth Gabbro (Paces & Miller 1993). Data have been processed using SQUID (Ludwig 2000) and plots prepared using ISOPLOT (Ludwig 1999). The $^{207}Pb/^{206}Pb$ ages have been used in the probability density spectra for areas older than 800 Ma, whereas for zircons <800 Ma the $^{206}Pb/^{238}U$ age is quoted. A number of areas analysed have been interpreted to be discordant and this has been based in part on the proximity to the concordia curve (using the total ratios, uncorrected for common Pb total), and in part on whether the radiogenic $^{206}Pb/^{238}U$ age is part of a grouping of like ages, or a single outlier significantly younger than the inferred depositional age of the sediment. Such interpreted discordant analyses have been excluded from the age spectra.

Both samples are dominated by zircons in the range 500–600 Ma (Figure 12). This prominent age peak comprises mostly zoned igneous zircon, but also includes minor but significant analyses of metamorphic zircon areas, as determined from the cathodoluminescence images. Such an age distribution is widely reported from Palaeozoic quartzose sandstone in eastern Australia and always a feature of Ordovician quartzose sandstones from the Lachlan Fold Belt (Ireland et al. 1998; Williams 1998; Fergusson &

Fanning 2002). Additionally, sample TH1 has a minor group of 7 zircons in the range 2670–2805 Ma. The detrital zircon ages for the youngest components (both igneous and metamorphic zircon) indicate that both samples are Ordovician or younger. They support the inference that the Girilambone Group is derived from metamorphism of Ordovician quartzose turbidite successions that are widespread throughout the Lachlan Fold Belt.

$^{40}Ar/^{39}Ar$ ages

Four samples were selected from the Girilambone Group for $^{40}Ar/^{39}Ar$ age analysis. Two samples are from the Girilambone district (Figure 2) and include a phyllitic psammite from near the lowest level of Hartmans Pit (Figure 4, sample H26) and a slate from drill core at Tritton (Figure 2, sample BDS029B – 372.1 m). Sample H26 contains well-developed S_2 differentiated layering folded about open folds with axial planar S_3 crenulation cleavage. Larger flakes of detrital muscovite occur in the rock. Sample BDS029B – 372.1 m is a sample of slate with a strong foliation defined by aligned muscovite with minor quartz and strongly recrystallised quartz-chlorite-calcite veins.

Samples of mica schist were taken from a road and a railway cutting to the east-southeast of Tottenham (Figure 8, samples TS6 and TS17). Both rocks have muscovite (0.2–0.3 mm) suitable for mineral separations, although some grains of muscovite are intergrown with chlorite. These outcrops have well developed S_2 differentiated layering which is strongly folded by F_{4A} folds with axial planar S_{4A} crenulation cleavage. Both samples have strong S_{4A} foliation with growth of new micas in this foliation. Sample TS17 also contains rare altered porphyroblasts replaced by chlorite and muscovite.

Sample BDS029B was crushed, sieved and washed in dilute nitric acid, deionised water and acetone. Approximately 20 mg of 0.5–1.0 mm whole rock chips were then handpicked, avoiding altered and/or iron-stained fragments. Due to the fine grain size and lower abundance of cleavage-forming white mica (relative to quartz) in sample H26, only coarser (detrital?) muscovite grains were separated from this sample for single-grain laser-probe analyses. The Tottenham samples had muscovite separates (180–200 μm) prepared using conventional magnetic and heavy liquid separation methods. A purity of greater than 99% was achieved by final handpicking of the muscovite. $^{40}Ar/^{39}Ar$ analyses were carried out at the School of Earth Sciences, University of Melbourne (see McDougall & Harrison 1999 for details of the techniques). Samples were irradiated along with flux monitor GA1550 biotite (Renne et al. 1998; age = 98.8 ± 0.5 Ma) in the McMaster University reactor, Canada. K_2SO_4 salts were also included in the irradiation package to determine correction factors for K-produced ^{40}Ar. After irradiation, weighed aliquots of samples TS6, TS17 and BD2029B were loaded into tin foil packets and step-heated in a tantalum resistance furnace. $^{40}Ar/^{39}Ar$ step-heating analyses were conducted on a VG3600 mass spectrometer, utilising a Daly detector. Single muscovite grains from sample H26 were step-heated using a defocused Nd-YAG laser, with isotopic analyses carried out on a MM5400 mass spectrometer and Daly detector. Mass discrimination values were monitored by analyses of purified air aliquots. Correction factors for interfering isotopes are: $(^{36}Ar/^{37}Ar)_{Ca} = 2.54\ (\pm 0.09) \times 10^{-4}$; $(^{39}Ar/^{37}Ar)_{Ca} = 6.51\ (\pm 0.31) \times 10^{-4}$ (Bottomley & York 1976); $(^{40}Ar/^{39}Ar)_K = 0.028 \pm 0.002$. Decay constants are those reported by Steiger and Jager (1977).

$^{40}Ar/^{39}Ar$ analytical results are shown in Table 3 and Figure 13. The isotopic data have been corrected for mass spectrometer backgrounds, mass discrimination and radioactive decay. Unless otherwise stated, ages are reported at one standard deviation and exclude the

uncertainties in the J-value, age of the standard and decay constants. Plateau ages are defined as comprising three or more consecutive heating steps representing >50% of the total $^{39}Ar_K$ released and with ages within 2σ of the weighted mean age (McDougall & Harrison 1999). Plateau ages are reported at the 2σ level, including the uncertainty in the J-error.

The two Tottenham samples, TS6 and TS17, yielded similar results, with both age spectra characterised by well-defined plateaux with weighted mean ages of 435.2 ± 2.6 Ma (2σ; MSWD = 0.71) and 440.2 ± 2.6 Ma (2σ; MSWD = 1.3), respectively (Figure 13a, b). The cause of the elevated apparent ages associated with some lower temperature steps in both samples is unclear, but could result from the presence of excess argon or minor (alteration-induced?) recoil loss of $^{39}Ar_K$. Given that higher metamorphic grades with biotite-bearing greenschist rocks occur only 7 km to the west-northwest and that rocks including sample TS17 contained retrogressed porphryoblasts of unknown minerals (probably cordierite), these ages are interpreted to indicate metamorphic cooling associated with some contractional deformation (S_{4A}) at around 435–440 Ma.

The BDS029B slate sample from Girilambone produced a more discordant age spectrum, with apparent ages generally increasing with increasing temperature from 206 ± 2 Ma to a maximum of 507 ± 3 Ma (Figure 13c). The younger low temperature ages are likely due to argon loss caused by minor alteration. The older high temperature ages are attributed to argon release from detrital muscovite grains. Although reasonably concordant, the intermediate temperature steps do not define a statistical age plateau, possibly due to minor $^{39}Ar_K$ recoil redistribution and increased contributions from detrital muscovite grains towards higher temperatures (Fergusson & Phillips 2001). These intermediate steps have a mean age of 434.3 ± 3.5 Ma (95% conf., weighted by √MSWD and including J-error), which is similar to ages obtained for the Tottenham samples, and is considered to represent a reasonable estimate for the time of cleavage formation in this slate. The significance of this foliation is not clear but its intensity and microstructure are consistent with it representing either S_1 or S_2 in the regional deformation succession.

Four coarse muscovite grains extracted from the Hartmans Pit sample (H26) were individually step-heated using the laser-probe (Table 4). Three grains produced similar results with ages of 480–490 Ma, which coincide with the younger U-Pb zircon ages. One grain yielded more discordant, older apparent ages averaging 562 ± 2 Ma. These results confirm the detrital character of the coarse muscovite grains in the slate samples and support the detrital zircon data.

DISCUSSION

Stratigraphic implications, depositional history and constraints on deformation

Constraints from the geochronology and lithology of the Girilambone Group are interpreted to indicate that the unit consists of a deformed and variably metamorphosed Early to late Middle Ordovician turbidite succession with minor mafic igneous rocks and bedded chert. We consider that evidence is insufficient to indicate the presence of a Cambrian metamorphic basement within the unit; instead we suggest that the unit has a variation in metamorphic grade. Iwata et al. (1995) used the term “Ballast Formation” for the low-grade part of the Girilambone Group although a map showing the contacts between the Ballast Formation and apparently higher-grade parts of the Girilambone Group has not been published.

The available age constraints from detrital zircons, detrital muscovites (reported herein) and conodont ages from bedded chert of the Ballast Formation (Iwata et al. 1995) indicates that deposition of the quartzose turbidite succession occurred at the same time as and almost certainly part of the gigantic Early to Middle Ordovician turbidite fan(s) of the Lachlan Fold Belt (VandenBerg & Stewart 1992). In contrast to the Ordovician turbidite deposits in Victoria no unambiguous mafic volcanic basement to the succession has been recognised within the Girilambone Zone. The mafic igneous rocks within the Girilambone Group are relatively restricted in distribution and do not have associated mappable pelagic units as found for basement to the Ordovician turbidites elsewhere (Fergusson 2003). Some of these mafic units are inferred to represent mafic intrusions within the unit (Fogarty 1996, 1998). The indications of widespread turbidite and pelagic deposition within the Girilambone Group, and its location adjacent to the Wagga-Omeo Zone, is considered consistent with an oceanic setting as part of the Wagga marginal sea (Powell 1984).

The timing of regional deformation of the Girilambone Group has been attributed to the Benambran Orogeny as indicated by regional relationships (MacRae 1987; Pogson 1991). Middle to Late Silurian plutonic rocks, southwest of Bobadah (Figure 1), intrude the Girilambone Group and truncate regional foliation within the unit indicating pre-Middle Silurian deformation, although in places these granites are strongly foliated indicating further regional deformation in the Middle to Late Silurian (MacRae 1987; Pogson 1991). Metamorphic clasts derived from the underlying Girilambone Group are abundant in Late Silurian conglomerate at the base of sedimentary and volcanic successions to the south of Tullamore (Figure 1; Sherwin 1996).

The $^{40}Ar/^{39}Ar$ ages of 435–440 Ma reported herein for the Girilambone Group in the Girilambone and Tottenham districts confirm earliest Silurian deformation and metamorphism for the Girilambone Group. These ages for the Tottenham district indicate timing of the later part of the deformation history (i.e. D_4 events) which was preceded by the recumbent folding event. The recumbent folding postdated an earlier event associated with the formation of a steeply dipping foliation presumably associated with horizontal contraction. The age of the Bulbodney Creek Intrusive Complex at 448 ± 4 Ma is marginally too old for the $^{40}Ar/^{39}Ar$ ages we have presented if the intrusion is considered to postdate deformation in the Girilambone Group.

Late Ordovician to Early Silurian subduction accretion

A major tectonic problem in the Lachlan Fold Belt is to account for the wide zone of deformation developed in the Girilambone and Wagga-Omeo Zones in the Late Ordovician to Early Silurian Benambran Orogeny (Powell 1984). Scheibner and Basden (1998) claimed that the Girilambone Group have an imbricate structure and intense deformation suggestive of a subduction complex setting, although they considered the possibility that Delamerian metamorphic basement, deformed in an accretionary subduction zone setting, was present in the unit. We have shown that no evidence exists for the presence of a Delamerian basement in the Girilambone Group. Scheibner and Basden (1998) appeared to favour the accretionary structure inferred for the Girilambone Group developing during closure of the Wagga marginal sea in the latest Ordovician by an east-dipping subduction zone under the Molong island arc.

Gray and Foster (1997) postulated three main subduction zones in the Lachlan Fold Belt two of which formed double divergent subduction zones responsible for the closure of the

Wagga marginal sea. The eastern of these double-divergent subduction zones was east-dipping and formed a subduction complex in the Tabberabbera Zone of eastern Victoria. In addition to the subduction complex interpretation of the Tabberabbera Zone, it was further suggested by Fergusson and Fanning (2002) and Fergusson (2003) that the central subprovince was dominated by one large subduction complex that formed the Girilambone, Wagga-Omeo and Tabberabbera Zones in the Late Ordovician to Early Silurian. Formation of the Girilambone Group as part of a subduction complex is difficult to evaluate given the lack of critical data on both the nature and timing of early deformation in this unit. Regional interpretations incorporating the subduction complex setting are considered below.

The reconstruction of Fergusson (2003), following Scheibner and Basden (1998), incorporated a subduction complex developed in the Girilambone Zone west of and related to east-dipping subduction that formed the late Middle to Late Ordovician part of the Molong island arc (Figure 14). This reconstruction is permissible given that the Girilambone Zone and the Molong island arc are adjacent to each other for at least 350 km (Figure 1) and no largescale strike-slip displacements have been demonstrated along their boundary. Major eastward thrusting of the Wagga-Omeo Zone over the Molong island arc is inferred from deep seismic data (Glen et al. 2001). Younger cover obscures the boundary between the greenschist to (?)amphibolite grade rocks of the eastern Girilambone Zone and the subgreenschist grade western part of the Molong island arc (Sherwin 1996) although the metamorphic differences between them are consistent with eastward thrusting as well.

We consider two alternatives related to this reconstruction (Figure 14). In the first alternative, subduction accretion in the Girilambone Group began synchronously with the initiation of widespread magmatic activity in the Molong island arc in the late Middle Ordovician (Glen et al. 1998). Formation of the subduction zone was closely followed by cessation of turbidite deposition, and deposition of the late Middle to Late Ordovician black shale unit that is widespread in the Wagga marginal sea (Fergusson & Fanning 2002) but absent from the Girilambone Group. Accretion in the eastern part of the Girilambone Zone would have overlapped with Darriwilian-Gisbornian chert deposition in the western part and also with deposition of the Upper Ordovician Murda Formation north of Condobolin (Scott 2000). In the second alternative, east-dipping subduction, and subduction accretion in the Girilambone Group, began in the latest Ordovician associated with final intrusive events in the Molong island arc at *ca* 440 Ma (Glen et al. 1998; Butera et al. 2001). Accretionary rocks at Batemans Bay and Narooma on the New South Wales south coast indicate west-dipping subduction to the east of the Molong island arc but this subduction may have been episodically active throughout the Late Ordovician to earliest Silurian interval (Fergusson & Frikken 2002). As noted by Fergusson (2003) it is unclear how subduction alternated from west- to east-dipping either side of the Molong island arc.

Regardless of which alternative is preferred, our model is that in the latest Ordovician to earliest Silurian the postulated subduction complex developed rapidly to the southwest from the Girilambone Zone through the Wagga-Omeo Zone. Late Ordovician black shale and even some Lower Silurian Yalmy Group equivalents occur in the Wagga-Omeo Zone (VandenBerg et al. 2000, p. 86) but much of the zone consists of the Early to Middle Ordovician turbidite succession. These younger rocks may have been deposited above the rapidly forming turbidite wedge and incorporated into it by subduction kneading. Both Gray and Foster (1997) and Collins and Hobbs (2001) attributed the Early to Middle Silurian plutonic belt in the Wagga-Omeo Zone to an easterly dipping subduction zone that formed the Tabberabbera Zone by subduction accretion. Rapid growth of the subduction complex and development of a thick turbidite, deforming wedge in the Wagga-Omeo Zone must have preceded development of the

plutonic belt, which was active at least by 425–430 Ma (Collins & Hobbs 2001). Both the subduction complex, incorporating the Girilambone, Wagga-Omeo and Tabberabbera Zones, and Molong island arc narrow southwards and apparently terminate in eastern Victoria (Figure 14). This arrangement partly reflects thrusting along their contacts (see above) but is potentially also caused by a southwards decrease in the amount of slip along the postulated east-dipping subduction zone.

Girilambone Zone and the Benambran Orogeny

As reviewed by Collins and Hobbs (2001) the Benambran Orogeny is a long-lived event with variable effects throughout the Lachlan Fold Belt. The early part of the deformation history of the Girilambone Zone is poorly known, mainly due to lack of data, and has been related to development of a subduction complex (see above). We have established that development of the D_2 deformation in the Girilambone region and D_2 and D_4 deformations in the Tottenham district are associated with greenschist to potentially local amphibolite grade metamorphism and have been dated at 435–440 Ma. This is presumably equivalent to D_2 deformation, and associated metamorphic segregation, reported by Scott and Lyons (2000) from the Girilambone Group in the Condobolin region. These deformations, and associated metamorphism, probably preceded development of the neighbouring plutonic belt in the Wagga-Omeo Zone (Collins & Hobbs 2001) and are considered part of the contractional deformation represented by the Benambran Orogeny. Deformation postdating regional greenschist metamorphism, such as the D_3 and D_4 events in the Girilambone region, late deformation in the southern domain of the Tottenham-Tullamore region and D_3 of Scott and Lyons in the Condobolin region, reflect continuing contractional deformation possibly in the later stages of the Benambran Orogeny although they may well be younger.

The structural history reported herein, for the Tottenham district, indicates greater complexity for the Benambran Orogeny than previously recognised. In the Tottenham district, the recumbent folding episode is atypical by comparison with steep structures developed elsewhere in association with the Benambran Orogeny. In many orogenic belts the association of low-angle ductile deformation fabrics, recumbent folds and exhumation of metamorphic rocks is attributed to extensional tectonics related to gravitational collapse and/or rollback in subduction related settings (Malavieille 1993; Ring et al. 1999). In the Tottenham district, no evidence for thrusting is recognised associated with this deformation (Figure 11) and an extensional origin accommodated by vertical flattening (i.e. pure shear) is considered a possibility. Ductile vertical flattening would have been potentially aided by enhanced heat flow in a region adjoining a recently active island arc (Figure 14).

In the Early Silurian (*ca* 435–440 Ma) at the time of deformation and cooling in the Tottenham district, in the reconstruction discussed above, the Girilambone Zone lay outboard from the recently active Molong island arc but in the inner part of the postulated subduction complex that was still growing rapidly southwest through the Tabberabbera Zone. In this context, a phase of extensional deformation is interpreted as a result of gravitational collapse in the older and presumably warmer part of the subduction complex perhaps aided by rollback in the adjoining subduction zone. The extensional deformation was apparently followed by contractional D_4 deformation and accompanying metamorphism, east-southeast of Tottenham, which preceded late Early Silurian development of the plutonic arc in the Wagga-Omeo Zone. Late contractional deformation associated with the development of the plutonic arc was

perhaps a reflection of collision between the Tabberabbera and Howqua River Zones (Fergusson 2003).

CONCLUSIONS

The Girilambone Group consists of a highly deformed Ordovician turbidite succession similar to other parts of the Lachlan Fold Belt. Reports of an older (Cambrian) metamorphic basement in the unit are unsubstantiated by our data. The eastern part of the Girilambone Group is a multiply deformed unit with several overprinting foliations. A strong differentiated layering is developed and has formed by crenulation of an earlier cleavage. Usually the differentiated layering (S_2) is postdated by one main crenulation cleavage axial planar to close to open folds. Southeast of Tottenham the differentiated layering is gently dipping due to abundant near-isoclinal recumbent folds.

Detrital zircons from two samples in the Girilambone district are dominated by ages in the interval 500–600 Ma consistent with other Ordovician turbidite units in the Lachlan Fold Belt. $^{40}Ar/^{39}Ar$ cooling ages from moderate grade metamorphic rocks around Tottenham indicate cooling at *ca* 435 Ma which is similar to a whole rock slate sample from the Tritton deposit 24 km to the southwest of Girilambone. These ages are consistent with contractional deformation as part of the Benambran Orogeny with possibly extensional deformation responsible for ductile thinning that produced recumbent folds in the main S_2 foliation in the Tottenham district.

The tectonic history of the Girilambone Group is difficult to decipher given the lack of exposure. We favour a model involving deposition as part of the gigantic Ordovician turbidite fan(s) in a marginal sea near East Gondwana and followed by disruption by intra-fold belt subduction zones. A subduction zone is inferred west of the Late Ordovician Molong island arc with growth of a subduction complex from northeast to southwest in the Girilambone Zone, followed by the Wagga-Omeo Zone in the latest Ordovician and subsequently by the Tabberabbera Zone in the Early Silurian. In the Early Silurian, the magmatic arc jumped southwest to form the north-northwest zone of elongate plutons in the Wagga-Omeo Zone.

ACKNOWLEDGEMENTS

This work was funded by the Australian Research Council (grant number A00103036) and supported by the University of Wollongong. Ann and Mike Fogarty are thanked for their hospitality at Nyngan. Mike Fogarty, formerly of Nord Pacific Ltd, kindly showed us many features of interest in the Girilambone region including the turbidites along the disused Nyngan-Bourke railway northwest of Girilambone. He also arranged access to the pits at the Girilambone Copper Mine and allowed us to sample drill core from the Tritton deposit. S. Sczcepanski is thanked for assistance with the $^{40}Ar/^{39}Ar$ analyses. Discussions with Mike Fogarty, Lawrie Sherwin, Evan Leitch and Leigh Schmidt are acknowledged. The Geological Survey of New South Wales kindly provided geophysical images for central New South Wales (courtesy of Dave Robson). Peter Johnson computer drafted the figures. Gordon Packham and Robin Offler are thanked for their thorough reviews of the manuscript.

REFERENCES

BOTTOMLEY, R. J. & YORK, D. 1976. Precision of the ^{40}Ar-^{39}Ar dating technique. *Earth and Planetary Science Letters* **9**, 39-44.

BUTERA K. M., WILLIAMS I. S., BLEVIN P. L. & SIMPSON C. J. 2001. Zircon U-Pb dating of Early Palaeozoic monzonitic intrusives from the Goonumbla area, New South Wales. *Australian Journal of Earth Sciences* **48**, 457-464.

COLLINS W. J. & HOBBS B. E. 2001. What caused the Early Silurian change from mafic to silicic (S-type) magmatism in the eastern Lachlan Fold Belt? *Australian Journal of Earth Sciences* **48**, 25–41.

FELTON E. A. 1978. *Geology of the Canbelego 1:100,000 Sheet 8134.* Geological Survey of New South Wales, Department of Mineral Resources, 171 p.

FERGUSSON C. L. 2003. Ordovician–Silurian accretion tectonics of the Lachlan Fold Belt, southeastern Australia. *Australian Journal of Earth Sciences* **50**, 475–490.

FERGUSSON C. L. & FANNING C. M. 2002. Late Ordovician stratigraphy, zircon provenance and tectonics, Lachlan Fold Belt, southeastern Australia. *Australian Journal of Earth Sciences* **49**, 423–436.

FERGUSSON C. L. & FRIKKEN P. 2002. Diapirism and structural thickening in an Early Palaeozoic subduction complex, southeastern New South Wales, Australia. *Journal of Structural Geology* **25**, 43-58.

FERGUSSON C. L. & PHILLIPS D. 2001. ^{40}Ar/^{39}Ar and K-Ar age constraints on the timing of regional deformation, south coast of New South Wales, Lachlan Fold Belt: problems and implications. *Australian Journal of Earth Sciences* **48**, 395-408.

FLEMING G., HICKS M. AND BARRON L. 2001. *Cobar basement study First programme of shallow reconnaissance aircore drilling, Sussex area, Cobar NSW.* Geological Survey of New South Wales, Department of Mineral Resources, Record GS2001/200.

FOGARTY J. M. 1996. Exploration for leachable copper deposits Girilambone district central west New South Wales. *In*: Cook W. G., Ford A. J. H., McDermott J. J., Standish P. N., Stegman C. L. & Stegman T. M. eds. *The Cobar Mineral Field — A 1996 Perspective*, pp. 179–193. Australasian Institute of Mining and Metallurgy, Spectrum Series **3/96**.

FOGARTY J. M. 1998. Girilambone district copper deposits. *In*: Berkman D. A. & Mackenzie D. H. eds. *Geology of Australian and Papua New Guinean Mineral Deposits*, pp. 593–600. Australasian Institute of Mining and Metallurgy, Melbourne.

GLEN R. A., WALSHE J. L., BARRON L. M. & WATKINS J. J. 1998. Ordovician convergent-margin volcanism and tectonism in the Lachlan sector of east Gondwana. *Geology* **26**, 751–754.

GLEN R. A., KORSCH R. J., DIREEN N. G., JONES L. E. A., JOHNSTONE D. W., LAWRIE K. C., FINLAYSON D. M. & SHAW R. D. 2002. Crustal structure of the Ordovician Macquarie Arc, eastern Lachlan Orogen, based on seismic reflection profiling. *Australian Journal of Earth Sciences* **49**, 323–348.

GRAY D. R. 1979. Geometry of crenulation-folds and their relationship to crenulation cleavage. *Journal of Structural Geology* **1**, 187–205.

GRAY D. R. 1997. Tectonics of the southeastern Australian Lachlan Fold Belt: structural and thermal aspects. *In*: Burg J. P. & Ford M. eds. *Orogeny through time*, pp. 149–177. Geological Society of London Special Publication **121**.

GRAY D. R. & FOSTER, D. A. 1997. Orogenic concepts—application and definition: Lachlan Fold Belt, eastern Australia. *American Journal of Science* **297**, 859–891.

IRELAND T. R., FLÖTTMANN T., FANNING C. M., GIBSON G. M. & PREISS W. V. 1998. Development of the early Paleozoic Pacific margin of Gondwana from detrital-zircon ages across the Delamerian orogen. *Geology* **26**, 243–246.

IWATA K., SCHMIDT B. L., LEITCH E. C., ALLAN A. D. & WATANABE T. 1995. Ordovician fossils from the Ballast Formation (Girilambone Group) of New South Wales. *Australian Journal of Earth Sciences* **42**, 371–376.

KEVRON GEOPHYSICS PTY LTD 1995a. *Nyngan SH55-15, Narromine SI55-03 Total Magnetic Intensity.* New South Wales Department of Mineral Resources.

KEVRON GEOPHYSICS PTY LTD 1995b. *Nyngan SH55-15, Narromine SI55-03 Radiometric Composite.* New South Wales Department of Mineral Resources.

LUDWIG K. R. 1999. *User's manual for Isoplot/Ex, Version 2.10, A geochronological toolkit for Microsoft Excel.* Berkeley Geochronology Center Special Publication No. 1a, 2455 Ridge Road, Berkeley CA 94709, USA.

LUDWIG K. R. 2000. *SQUID 1.00, A User's Manual; Berkeley Geochronology Center Special Publication.* No. 2, 2455 Ridge Road, Berkeley, CA 94709, USA.

MACRAE G. P. 1987. *Geology of the Nymagee 1:100 000 sheet 8133.* Geological Survey of New South Wales, Department of Mineral Resources, 137 p.

MALAVIEILLE J. 1993. Late orogenic extension in mountain belts: insights from the Basin and Range and the Late Paleozoic Variscan Belt. *Tectonics* **12**, 1115–1130.

MCDOUGALL I. & HARRISON T. M. 1999. *Geochronology and thermochronology by the $^{40}Ar/^{39}Ar$ method.* Second Edition. Oxford University Press, New York.

PACES J. B. & MILLER J. D. 1993. Precise U–Pb ages of Duluth Complex and related mafic intrusions, northeastern Minnesota: Geochronological insights to physical, petrogenetic, paleomagnetic, and tectonomagmatic processes associated with the 1.1 Ga Midcontinent Rift System. *Journal of Geophysical Research* **98**, 13997–14013.

POGSON D. J. 1991. *Geology of the Bobadah 1:100 000 sheet 8233*. Geological Survey of New South Wales, Department of Minerals and Energy, 130 p.

POWELL C. MCA. 1984. Ordovician to earliest Silurian: marginal sea and island arc; Silurian to mid-Devonian dextral transtensional margin; Late Devonian and Early Carboniferous: continental magmatic arc along the eastern edge of the Lachlan Fold Belt. *In*: Veevers J. J. ed. *Phanerozoic Earth History of Australia*, pp. 290–340. Oxford University Press, Oxford.

RENNE P. R., SWISHER C. C. DEINO A. L. KARNER D. B. OWENS T. L. & DEPAOLO D. J. 1998. Intercalibration of standards, absolute ages and uncertainties in $^{40}Ar/^{39}Ar$ dating. *Chemical Geology* **145**, 117–152.

RING U., BRANDON M. T., WILLETT S. D. & LISTER G. S. 1999. Exhumation processes. *In*: Ring. U., Brandon M. T., Willet S. D. & Lister G. S. eds, *Exhumation Processes, Normal Faulting, Ductile Flow and Erosion,* pp. 1–27. Geological Society, London, Special Publication **154**.

SCHEIBNER E. & BASDEN H. ed. 1998. *Geology of New South Wales - Synthesis. Volume 2 Geological Evolution.* Geological Survey of New South Wales, Memoir 13(2), 666 p.

SCOTT M. M. 2000. Murda Formation (Ogm). *In*: Lyons P., Raymond O. L. & Duggen M. B. eds. *Forbes 1:250 000 Geological Sheet SI55-7, 2nd edition, Explanatory Notes,* p 17. AGSO Record 2000/20.

SCOTT M. M. & LYONS P. 2000. Girilabone Group (Og). *In*: Lyons P., Raymond O. L. & Duggen M. B. eds. *Forbes 1:250 000 Geological Sheet SI55-7, 2nd edition, Explanatory Notes,* p 13-16. AGSO Record 2000/20.

SHERWIN L. 1996. *Narromine 1:250 000 Geological Sheet SI/55-3: Explanatory Notes*. Geological Survey of New South Wales.

SHIELDS P. 1996. Geology of the Girilambone Copper Deposit. *In*: Cook W. G., Ford A. J. H., McDermott J. J., Standish P. N., Stegman C. L. & Stegman T. M. eds. *The Cobar Mineral Field — A 1996 Perspective,* pp. 293–304. Australasian Institute of Mining and

Metallurgy, Spectrum Series **3/96**.

SMITH E. A. 1971. *Report of the exploration of Exploration Licence 287, Nyngan, NSW to July 31st 1971.* Geological Survey of New South Wales, open file report GS 1971/655 (unpublished).

STEIGER R. H. & JAGER E. 1977. Subcommission on geochronology: Convention on the use of decay constants in geo- and cosmochronology. *Earth and Planetary Science Letters* **36**, 359–362.

STEWART I. R. & GLEN R. A. 1986. An Ordovician age for part of the Girilambone Group at Yanda Creek, east of Cobar. *Quarterly Notes of the Geological Survey of New South Wales* **64**, 23–25.

SUPPEL D. W. 1975. Girilambone Anticlinorial Zone. *In*: Markham N. L. & Basden H. eds. *The Mineral Deposits of New South Wales,* pp. 118–131. Geological Survey of New South Wales, Sydney.

TESLA AIRBORNE GEOSCIENCE PTY LTD 1999a. *Cobar SH55/14 – Nymagee SI55/02 TMI reduced to the pole.* New South Wales Department of Mineral Resources.

TESLA AIRBORNE GEOSCIENCE PTY LTD 1999b. *Cobar SH55/14 – Nymagee SI55/02 K/Th/U composite.* New South Wales Department of Mineral Resources.

VANDENBERG A. H. M. & STEWART I. R. 1992. Ordovician terranes of the southeastern Lachlan Fold Belt: stratigraphy, structure and palaeogeographic reconstruction. *Tectonophysics* **214**, 159–176.

VANDENBERG A. H. M., WILLMAN C. E., MAHER S., SIMONS B. A., CAYLEY R. A., TAYLOR D. H., MORAND V. J., MOORE D. H. & RADOJKOVIC A. 2000. *The Tasman Fold Belt System in Victoria. Geology and mineralisation of Proterozoic to Carboniferous rocks.* Geological Survey of Victoria Special Publication.

WILLIAMS I. S. 1998. U-Th-Pb Geochronology by Ion Microprobe. *In*: McKibben M. A., Shanks III W. C. & Ridley W. I. Eds. *Applications of microanalytical techniques to understanding mineralizing processes*. *Reviews in Economic Geology* **7**, 1–35.

YARDLEY B. W. D. 1989. *An Introduction to Metamorphic Petrology.* Longman Scientific & Technical, Harrow, UK, 248 p.

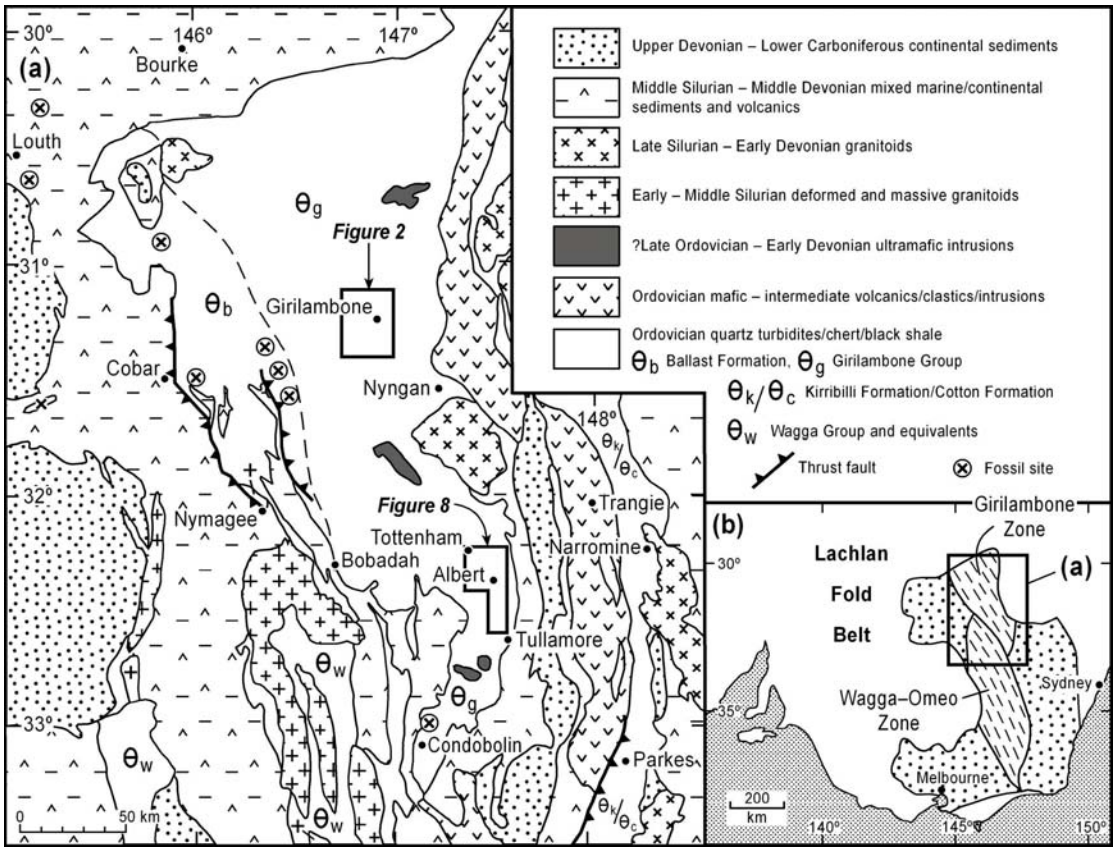

Figure 1 (a) Regional geology of central New South Wales (Lachlan Fold Belt). Post-Carboniferous (mainly Cenozoic) cover is not shown. Insets shows locations of Figures 2 and 8. (b) Location of (a) in mainland southeast Australia.

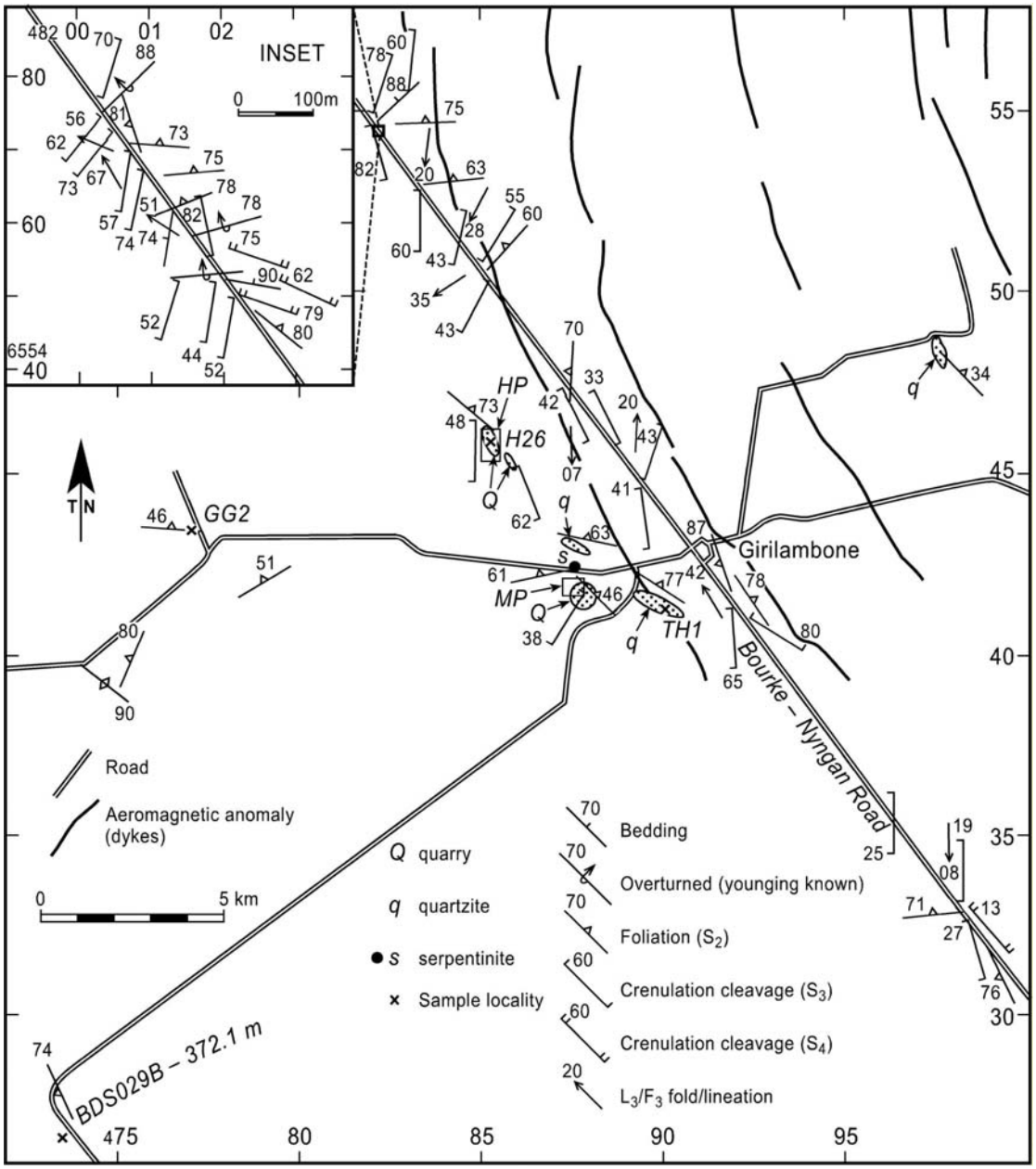

Figure 2 Map of the bedrock geology (Girilambone Group) in the Girilambone district. See Figure 1 for location. Inset shows enlargement of structures measured in the cutting 14.5 km northwest of Girilambone on the disused Nyngan-Bourke railway line. More detailed maps are shown in Figure 4 for Hartmans Pit (HP) and in Figure 5 for the northwest part of the Murrawombie Pit (MP). Detrital zircon U-Pb ages were determined for samples TH1 (quartzite) and GG2 (psammite). $^{40}Ar/^{39}Ar$ ages were determined for samples H26 (psammitic phyllite) and BDS-029B (slate).

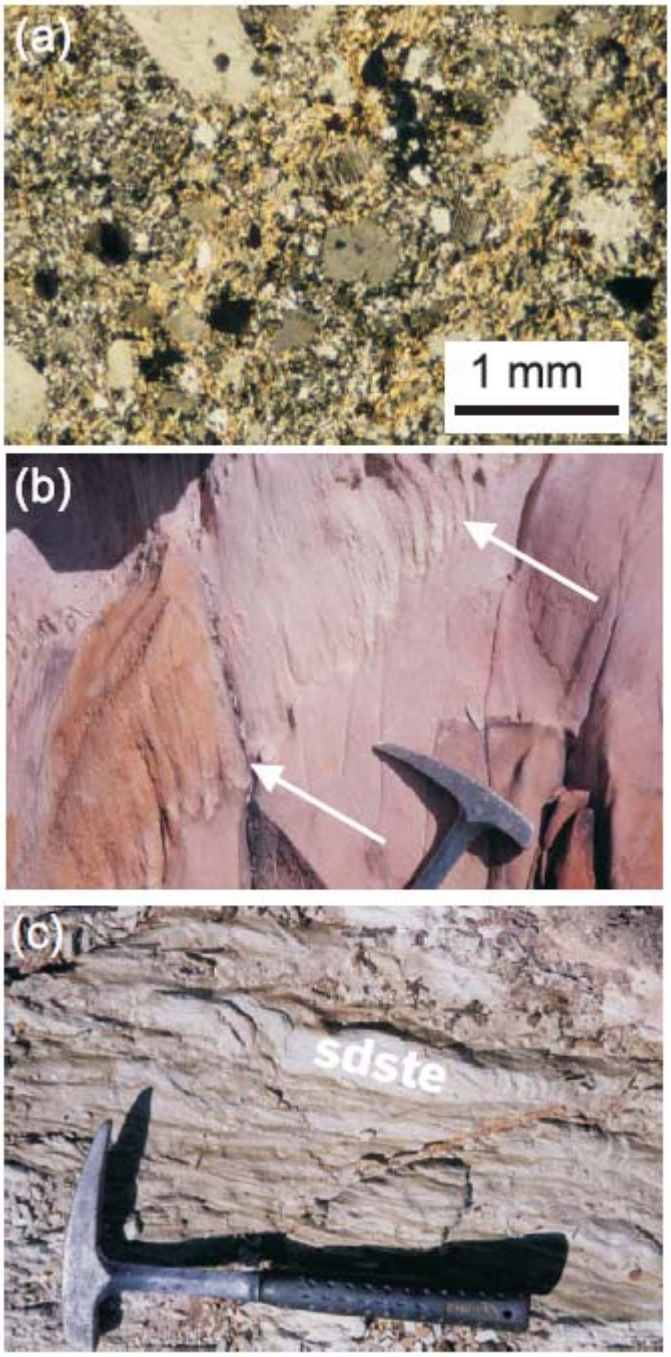

Figure 3 Sedimentary features in Girilambone Group around Girilambone. (a) Psammite (Sample GG2) with relict detrital quartz grains in an abundant very fine-grained matrix mainly of quartz with muscovite and chlorite (0477044 6543514 Coolabah (8235) 1:100 000 sheet). Cross polarised light. (b) Loadcasts at the base of a psammite layer (arrows), from a cutting in the disused Nyngan-Bourke railway line, 14.5 km northwest of Girilambone (0482038 6554749 Coolabah (8235) 1:100 000 sheet). (c) Thin alternating layers of fine sandstone (sdste, some with Bouma C micro-crosslamination) and mudstone, from a cutting in the disused Nyngan-Bourke railway line, 14.5 km northwest of Girilambone (0482201 6554534 Coolabah (8235) 1:100 000 sheet).

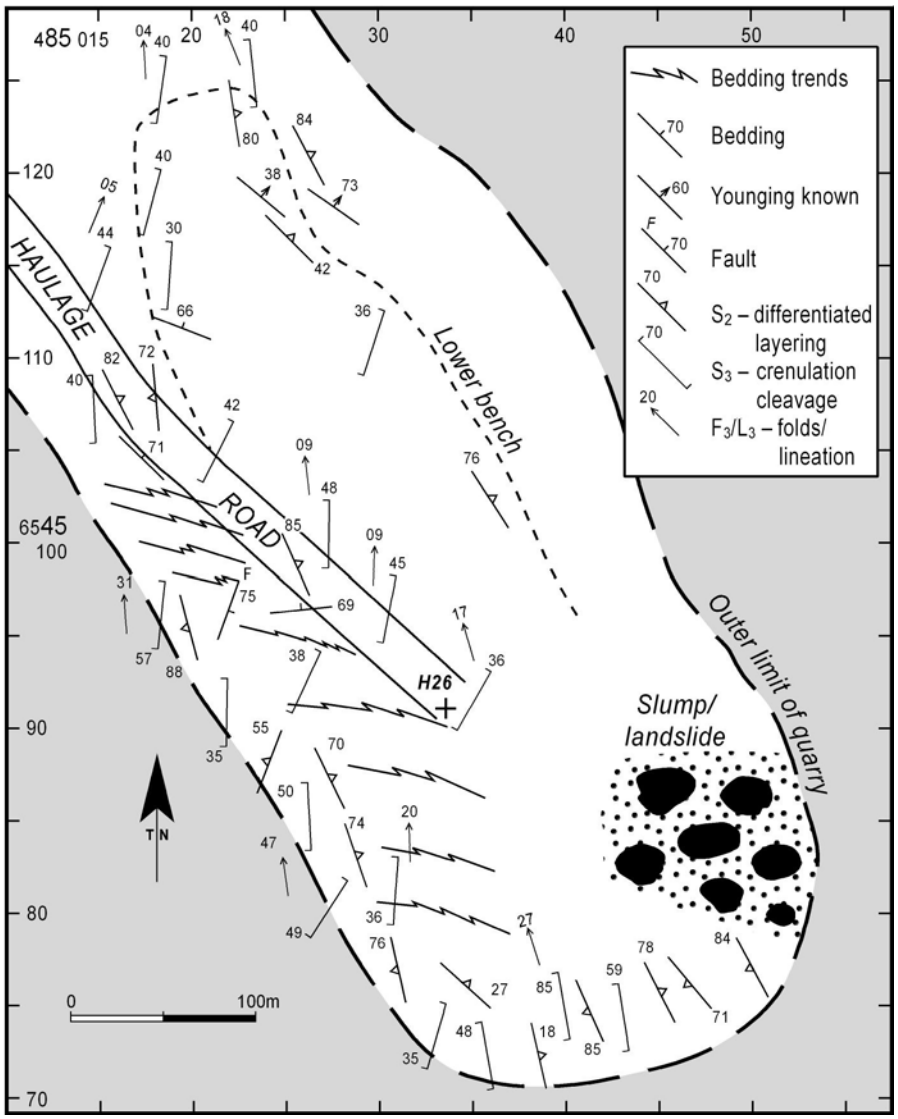

Figure 4 Detailed map of the central and southern parts of Hartmans Pit, northern part of the Girilambone Copper Mine. Map of the pit has been constructed from GPS measurements made from a portable GPS device. See Figure 2 for location. Cross with H26 is the sample site for $^{40}Ar/^{39}Ar$ detrital muscovite ages. Note bedding trends are idealised and affected by many small folds (shown schematically only).

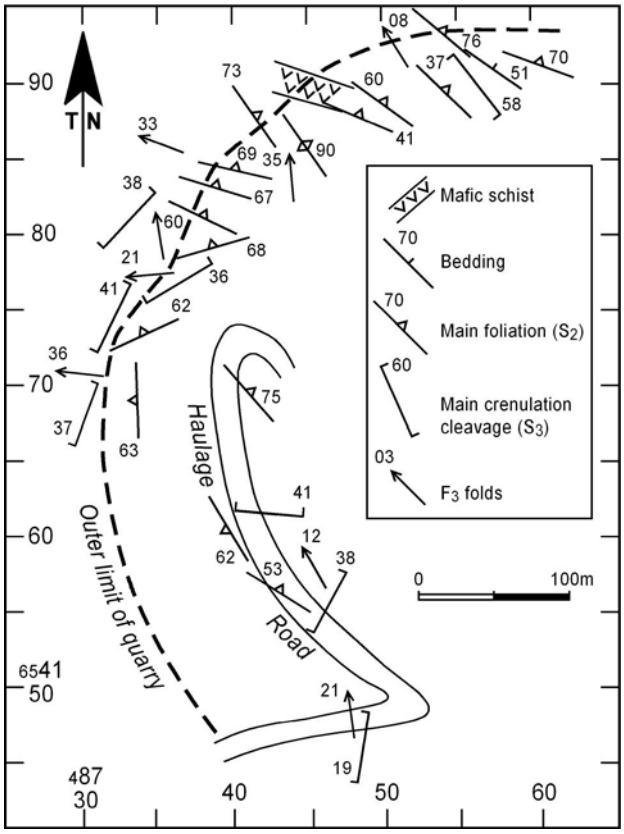

Figure 5 Northeastern section of Murrawombie Pit, Girilambone Copper Mine. Map of the pit has been constructed from GPS measurements made from a portable GPS device. See Figure 2 for location.

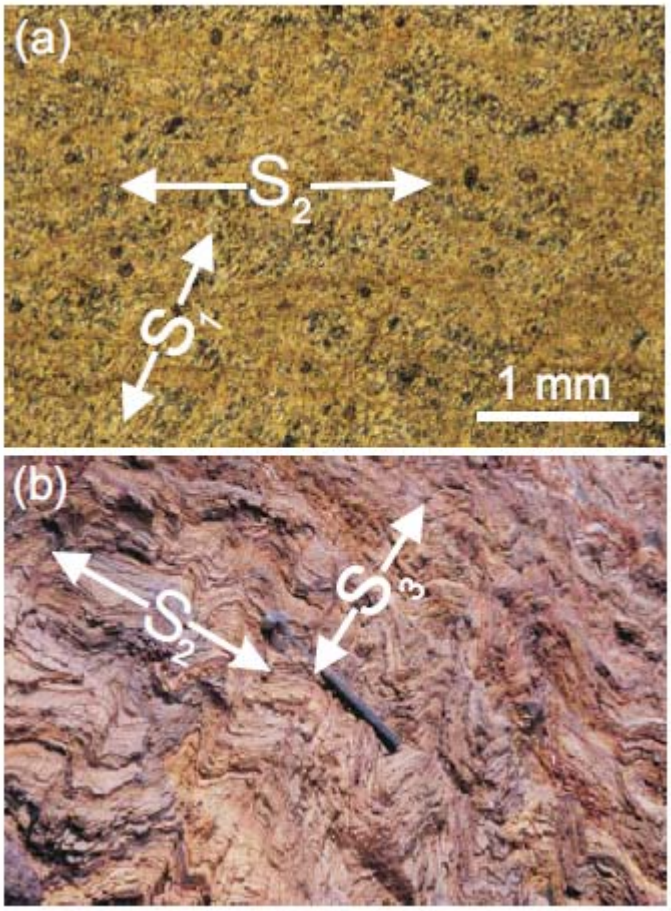

Figure 6 Photographs of structures in the Girilambone district. (a) Differentiated S_2 crenulation cleavage with relict S_1 in the quartz-rich microlithon (thin section of Sample G25M, 0482148 6554609 Coolabah (8235) 1:100 000 sheet). Cross polarised light. (b) S_3 crenulation cleavage axial planar to open F_3 folds. Hartmans Pit (0485221 6545943 Coolabah (8235) 1:100 000 sheet). Hammer 33 cm long.

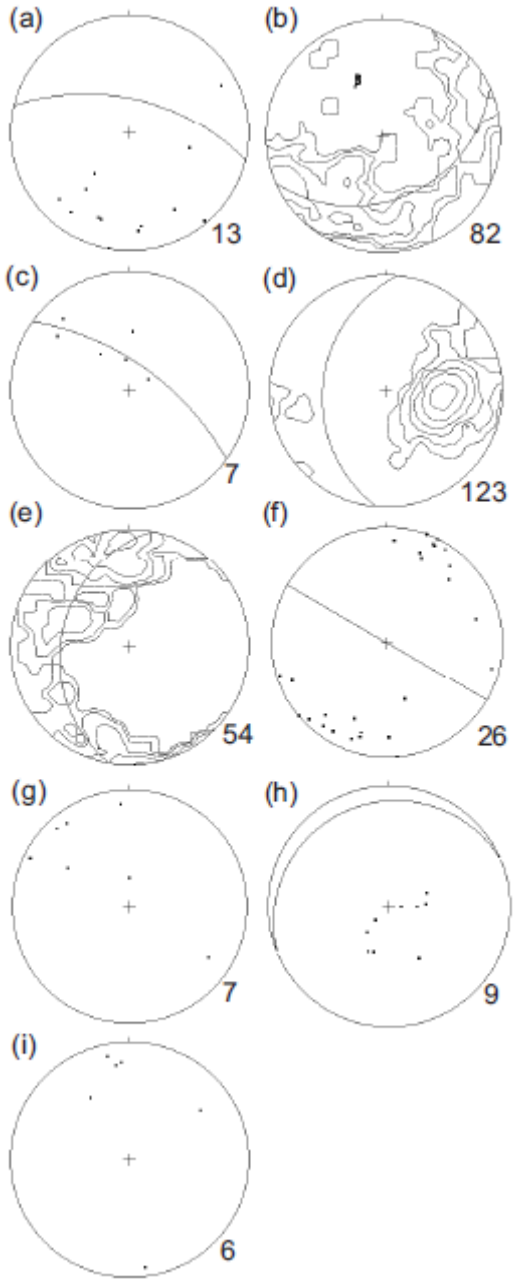

Figure 7 Lower hemisphere equal area stereographic projections of structural data from the Girilambone district. Number of measurements shown at lower right of each stereonet. (a) Poles to bedding. (b) Poles to S_2, contoured at 1, 2, 4 and 8% per 1% area, β-axis 46º/336º. (c) L_2 – girdle 72º/036º. (d) Poles to S_3, contoured at 1, 2, 4 and 8% per 1% area, mean 44º/275º. (e) L_3, contoured at 1, 2, 4, 8 and 16% per 1% area, girdle is 42º/280º, mean 18º/349º. (f) Poles to S_{4A} – mean 88º/030º. (g) F_{4A} – mean 16º/317º. (h) Poles to S_{4B}. (i) L_{4B}.

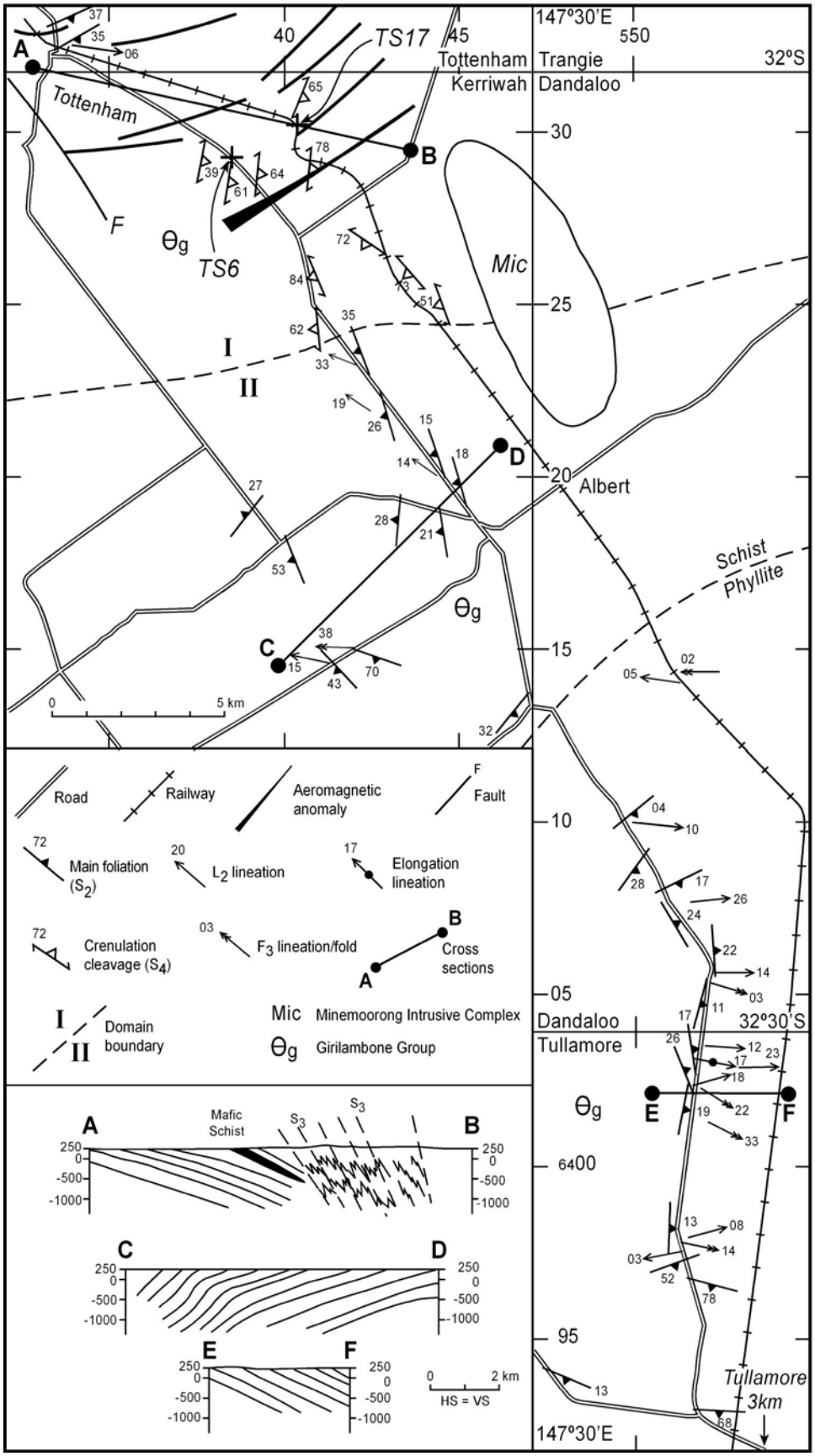
147°30'E
550
Tottenham
Trangie
32°S
Kerriwah
Dandaloo
TS17
TS6
Tottenham
F
Θg
Mic
A
B
C
D
E
F
I
II
Albert
Schist
Phyllite
Dandaloo
32°30'S
Tullamore
Tullamore
3km
147°30'E
0
5 km
Road
Railway
Aeromagnetic anomaly
Fault
Main foliation (S2)
L2 lineation
Elongation lineation
Crenulation cleavage (S4)
F3 lineation/fold
Cross sections
Domain boundary
Mic Minemoorong Intrusive Complex
Θg Girilambone Group
Mafic Schist
S3
HS = VS
0
2 km

Figure 8 Map and cross sections of the bedrock geology for the region to the south of Tottenham. See Figure 1 for location. Aeromagnetic anomalies interpreted from Nyngan Total Magnetic Image (Kevron Geophysics Pty Ltd 1995a) indicate the location of mafic schist and quartz-magnetite rocks as shown by changes in soil type, float and old mines. Fault to the south of Tottenham is based on interpretation of the magnetic image. $^{40}Ar/^{39}Ar$ ages were determined for samples TS6 and TS17. Mafic schist occurs in a railway cutting located on magnetic anomaly immediately south of sample site TS17.

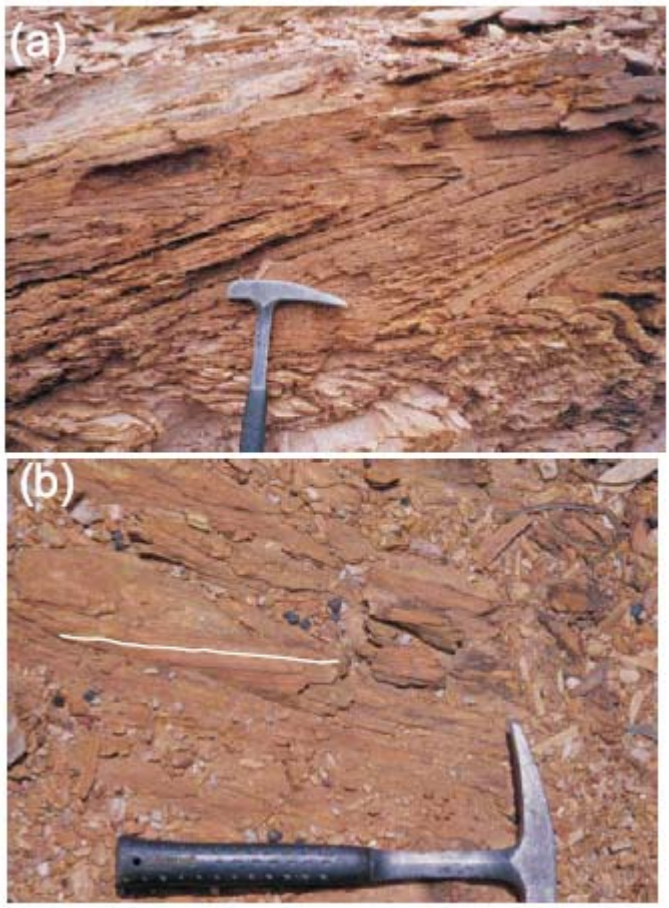

Figure 9 Photographs of structures in the Tottenham district. (a) Siliceous phyllite showing recumbent F_3 folds, railway cutting southeast of Albert (0551136 6414261 Dandaloo (8433-II & III) 1:50 000 sheet). (b) Flat pavement of a road surface displaying an intersection lineation (L_2) folded around an F_3 fold hinge (shown by white line, 0551175 6397654 Tullamore (8432-I & IV) 1:50 000 sheet).

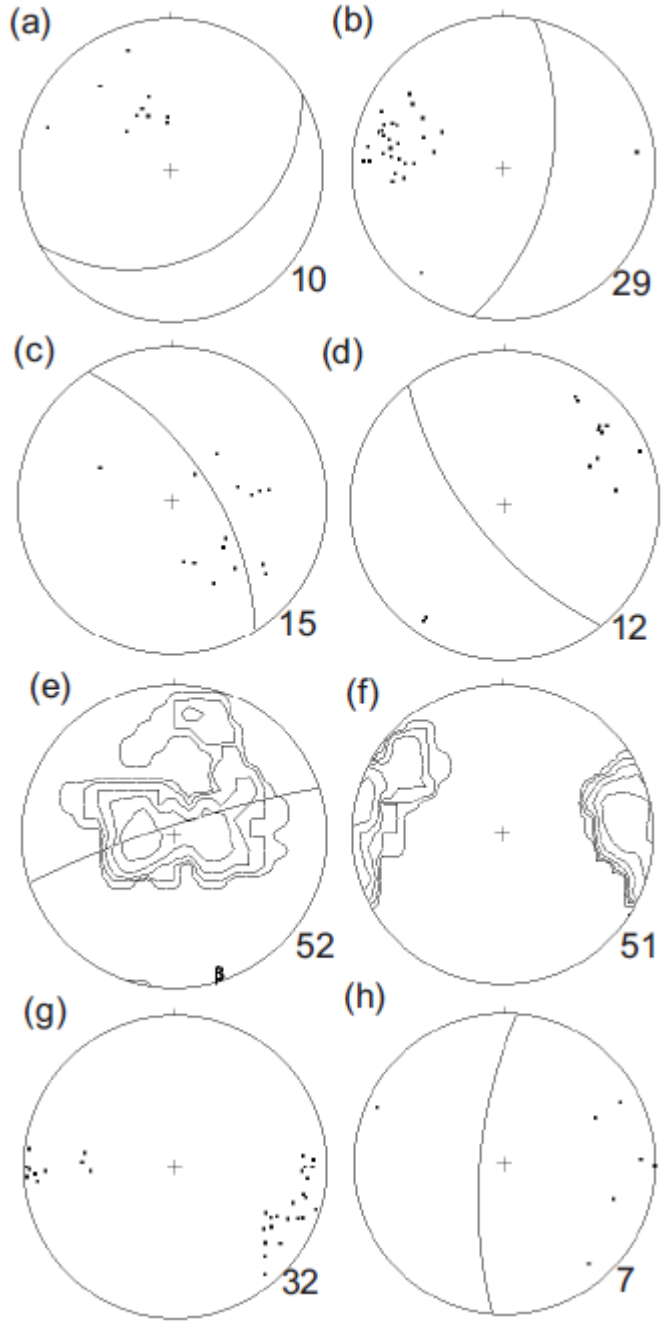

Figure 10 Lower hemisphere equal area stereographic projections of structural data from the Tottenham district. Number of measurements shown at lower right of each stereonet. (a)–(d) Structures in domain I (northern part of the Tottenham district). (a) Poles to S_2. (b) Poles to S_{4A} – mean 64º/102º. (c) L_{4A} – girdle 68º/057º. (d) Poles to S_{4B}. (e)–(h) Structures in domain II (southern part of the Tottenham district). (e) Poles to S_2 contoured at 1, 2, 4, 8 and 16% per 1% area, β-axis 06º/162º, mean 06º/149º. (f) L_2 contoured at 1, 2, 4, 8 and 16% per 1% area, mean 06º/192º. (g) F_3 – mean 09º/104º. (h) Poles to AP4.

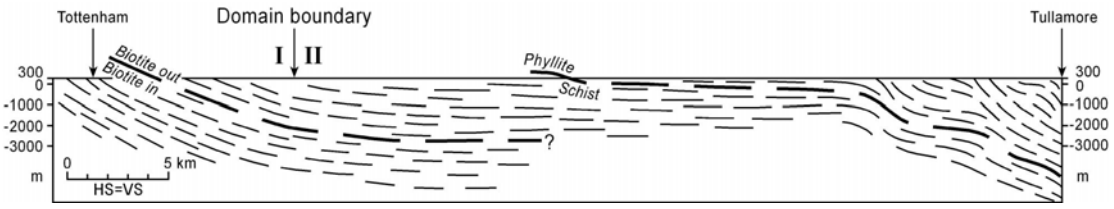

Figure 11 Cross section between Tottenham and Tullamore showing the relationship between the main S_2/S_3 foliation and changes in rock type and metamorphic grade. Note that the D_4 structures 7 km east-southeast of Tottenham have not been projected onto the cross section as they are only slightly oblique to the cross section location. Folds in S_2/S_3 north of Tullamore are open to broad late east-west trending folds. See Figure 1 for locations of Tullamore and Tottenham.

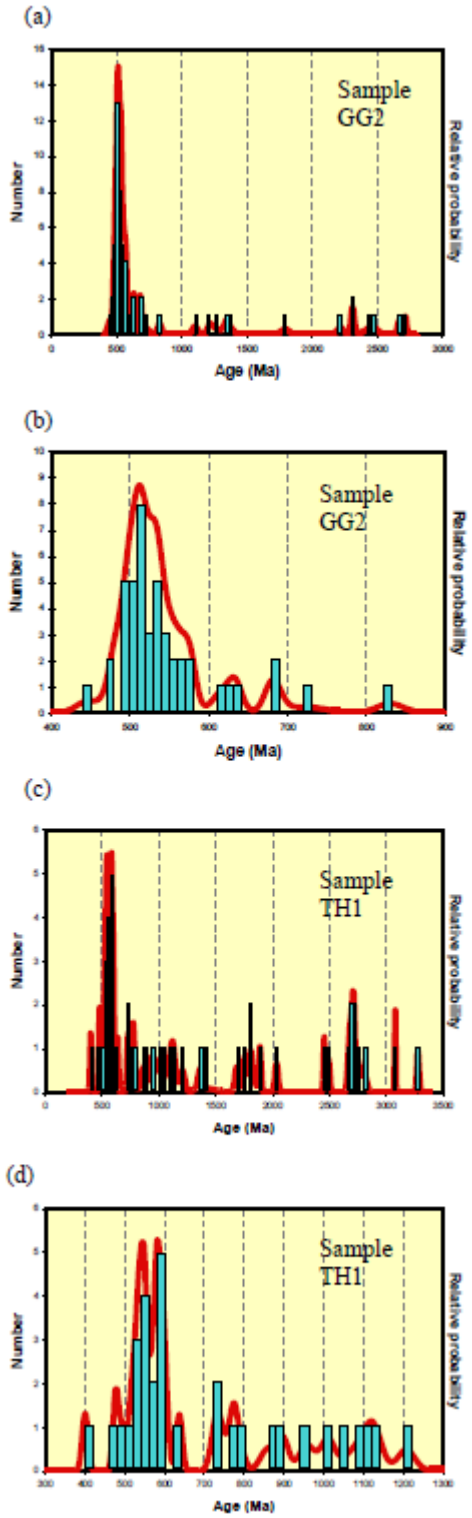

Figure 12 Combined histograms and probability density distribution of detrital-zircon age spectra for samples of psammite GG2 (a-b) and quartzite TH1 (c-d) from the Girilambone Group in the Girilambone district. For locations see Figure 2.

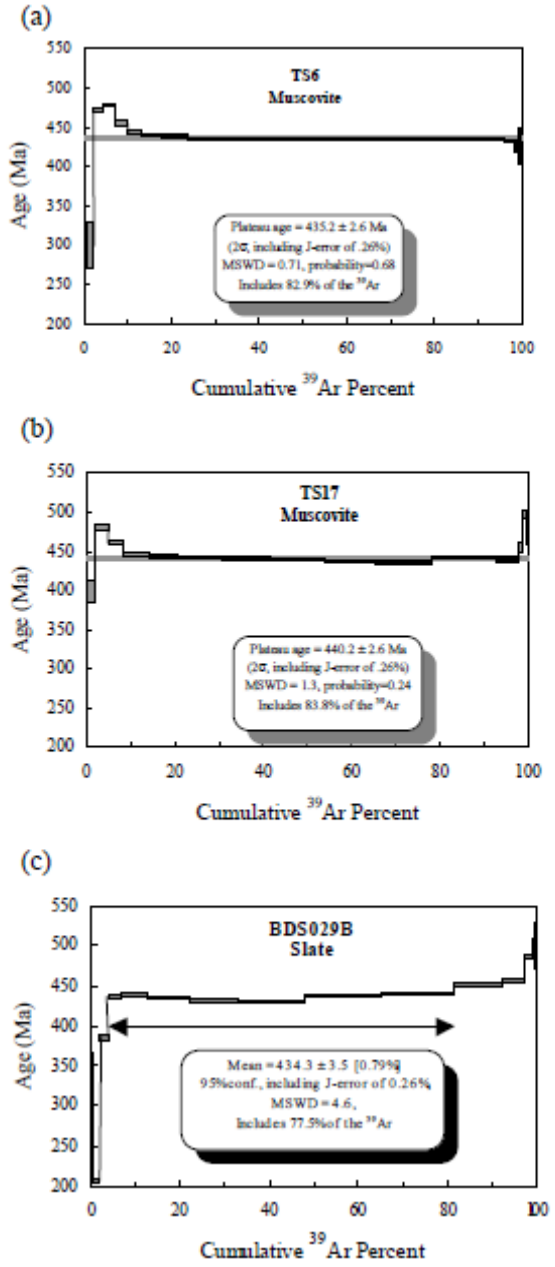

Figure 13 $^{40}Ar/^{39}Ar$ step heating spectra for muscovite and whole-rock slate chips from Girilambone Group samples. (a) Sample TS6 from near Tottenham (see Figure 8 for location). (b) Sample TS17 from near Tottenham (see Figure 8 for location). (c) Sample BDS029B from drill core at Tritton (see Figure 2 for location).

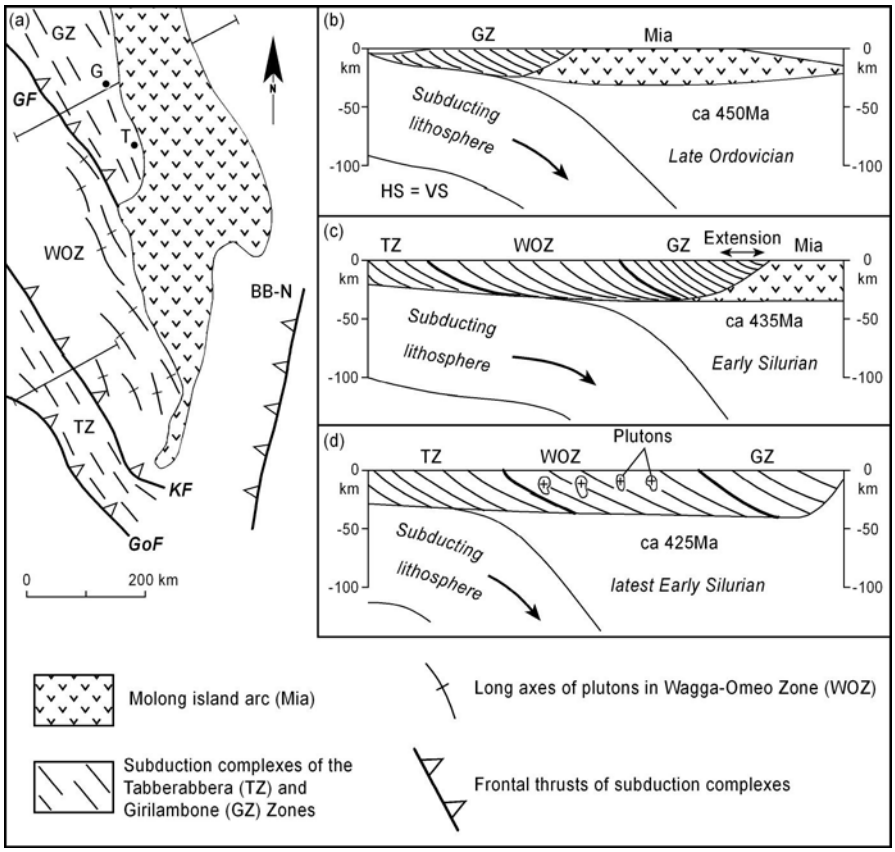

Figure 14 (a) Tectonic elements of the central and eastern subprovinces of the Lachlan Fold Belt (map of present geometry). Lines show location of all cross sections in (b)–(d). (b) Cross section for the Late Ordovician at *ca* 450 Ma showing an east-dipping subduction zone under the Girilambone Zone and the Molong island arc. (c) Cross section for the Early Silurian at *ca* 435 Ma showing an east-dipping subduction zone under the Molong island arc, Girilambone, Wagga-Omeo and Tabberabbera Zones. Note extensional deformation occurred in the eastern Girilambone Zone at this time. (d) Cross section for the latest Early Silurian at *ca* 425 Ma showing an east-dipping subduction zone under the Girilambone, Wagga-Omeo and Tabberabbera Zones. Note plutons in the Wagga-Omeo Zone. Abbreviations: BB-N = Batemans Bay and Narooma subduction complex, GF = Gilmore Fault, G = Girilambone, GZ = Girilambone Zone, GoF = Governor Fault, KF = Kiewa Fault, M = Molong, Mia = Molong island arc, TZ = Tabberabbera Zone, T = Tottenham, WOZ = Wagga-Omeo Zone.

TABLES

Table 1 Summary of SHRIMP U-Pb zircon results for sample GG2.

Table 1. Summary of SHRIMP U-Pb zircon results for sample GG2.

							Total Ratios				Radiogenic Ratios							Age (Ma)				
Grain	U	Th	Th/U	Pb*	^{204}Pb/	f_{206}	^{238}U/		^{207}Pb/		^{206}Pb/		^{207}Pb/		^{207}Pb/			^{206}Pb/		^{207}Pb/		%
spot	(ppm)	(ppm)		(ppm)	^{206}Pb	%	^{206}Pb	±	^{206}Pb		^{238}U	±	^{235}U		^{206}Pb	±	ρ	^{238}U	±	^{206}Pb	±	Disc
1.1	322	130	0.41	25.4	-	<0.01	10.901	0.175	0.0627	0.0015	0.0921	0.0015						568	9			
2.1	77	69	0.89	14.4	-	<0.01	4.601	0.129	0.0804	0.0024	0.2174	0.0061	2.413	0.099	0.0805	0.0024	0.683	1268	32	1209	59	-5
3.1	393	87	0.22	30.9	0.000734	1.32	10.943	0.189	0.0664	0.0014	0.0902	0.0017						557	10			
4.1	388	429		28.0	0.000712	1.29	11.913	0.189	0.0640	0.0015	0.0829	0.0014						513	9			
5.1	416	213		31.9	0.001141	2.07	11.211	0.175	0.0704	0.0015	0.0874	0.0015						540	9			
6.1	231	189	0.82	16.7	0.000000	0.00	11.913	0.261	0.0613	0.0043	0.0839	0.0018						520	11			
7.1	324	58	0.18	26.0	-	<0.01	10.729	0.172	0.0595	0.0014	0.0933	0.0015						575	9			
8.1	587	20	0.03	56.6	0.000425	0.75	8.918	0.127	0.0667	0.0010	0.1113	0.0016						680	9			
9.1	129	120	0.93	9.7	-	<0.01	11.393	0.298	0.0660	0.0025	0.0879	0.0023						543	14			
10	158	196	1.25	37.3	0.008486	13.98	3.633	0.061	0.2048	0.0025	0.2368	0.0059	2.800	0.750	0.0858	0.0229	0.094	1370	31	1333	516	-3
11	321	189	0.59	63.6	0.000082	0.14	4.338	0.061	0.0793	0.0011	0.2313	0.0033	2.611	0.052	0.0819	0.0011	0.713	1341	19	1243	27	-8
12	501	767	1.53	37.0	0.004180	7.01	11.630	0.166	0.1379	0.0020	0.0800	0.0014						496	8			
13	123	59	0.48	10.7	0.000095	0.17	9.797	0.221	0.0569	0.0023	0.1019	0.0023						625	14			
14	176	107	0.61	13.3	-	<0.01	11.336	0.220	0.0594	0.0020	0.0885	0.0017						547	10			
15	240	292	1.22	18.2	0.000162	0.29	11.306	0.197	0.0558	0.0016	0.0882	0.0016						545	9			
16	636	37	0.06	56.8	0.000320	0.57	9.623	0.126	0.0650	0.0012	0.1033	0.0014						634	8			
17	191	147	0.77	14.1	-	<0.01	11.661	0.222	0.0589	0.0019	0.0863	0.0017						534	10			
18	515	547	1.06	49.6	0.018611	30.16	8.918	0.118	0.3515	0.0059	0.0783	0.0028						486	17			
19	212	82	0.39	15.4	0.000493	0.89	11.834	0.215	0.0613	0.0018	0.0837	0.0015						518	9			
20	405	398	0.98	29.2	0.000762	1.40	11.894	0.200	0.0621	0.0016	0.0829	0.0015						513	9			
21	248	264	1.06	18.6	0.001150	2.15	11.460	0.217	0.0615	0.0019	0.0854	0.0018						528	10			
22	680	361	0.53	50.3	0.000192	0.34	11.621	0.189	0.0608	0.0013	0.0858	0.0014						530	8			
23	240	128	0.53	16.3	0.000082	0.15	12.634	0.387	0.0602	0.0029	0.0790	0.0025						490	15			
24	174	313	1.79	14.9	-	<0.01	10.047	0.219	0.0595	0.0021	0.1000	0.0022						615	13			
25	421	394	0.94	30.4	0.001458	2.54	11.903	0.202	0.0867	0.0028	0.0819	0.0015						507	9			
26	186	161	0.87	12.9	0.000614	1.15	12.379	0.286	0.0543	0.0023	0.0799	0.0020						495	12			
27	636	433	0.68	246.6	0.002082	2.97	2.218	0.031	0.1840	0.0012	0.4376	0.0063	9.507	0.301	0.1576	0.0044	0.457	2340	28	2430	48	4
28	502	320	0.64	37.5	0.001894	3.40	11.513	0.179	0.0841	0.0017	0.0839	0.0015						519	9			
29	89	21	0.24	34.5	0.000111	0.16	2.210	0.051	0.1624	0.0027	0.4518	0.0105	10.032	0.311	0.1610	0.0033	0.749	2403	47	2467	35	3
29	300	186	0.62	127.6	0.000005	0.01	2.022	0.030	0.1816	0.0014	0.4946	0.0074	12.376	0.212	0.1815	0.0015	0.872	2590	32	2667	14	3
30	517	494	0.96	36.7	0.000068	0.12	12.084	0.172	0.0584	0.0012	0.0827	0.0012						512	7			
31	338	99	0.29	150.0	0.000028	0.04	1.937	0.026	0.1871	0.0012	0.5161	0.0069	13.293	0.195	0.1868	0.0012	0.904	2683	29	2714	10	1
32	133	188	1.42	8.6	0.002984	4.95	13.281	0.361	0.1249	0.0038	0.0716	0.0024						446	14			
33	203	116	0.57	23.9	0.000024	0.04	7.276	0.159	0.0603	0.0016	0.1374	0.0030						830	17			
34	521	279	0.54	39.3	0.001516	2.69	11.393	0.157	0.0819	0.0019	0.0854	0.0013						528	7			
35	711	32	0.05	57.2	0.000019	0.03	10.675	0.136	0.0596	0.0009	0.0936	0.0012						577	7			
36	45	16	0.35	3.2	0.000443	0.79	12.232	0.411	0.0658	0.0040	0.0811	0.0033						503	20			
37	3888	5191	1.33	62.4	0.005430	6.06	53.497	0.974	0.4981	0.3046	0.0176	0.0004						112	2			
38	363	35	0.10	139.6	-	<0.01	2.231	0.029	0.1460	0.0010	0.4485	0.0059	9.067	0.135	0.1466	0.0010	0.881	2389	26	2307	12	-3
39	779	456	0.59	57.8	-	<0.01	11.577	0.145	0.2313	0.0020	0.0865	0.0011						535	6			
40	288	263	0.92	27.7	0.000194	0.32	8.924	0.157	0.0914	0.0023	0.1117	0.0020						683	12			
41	88	34	0.38	1.5	0.000625	1.16	50.936	2.028	0.0575	0.0054	0.0194	0.0010						124	6			
42	365	389	1.06	24.3	0.000147	0.23	12.932	0.198	0.1197	0.0020	0.0772	0.0012						479	7			
43	179	70	0.39	31.9	-	<0.01	4.818	0.080	0.0813	0.0014	0.2074	0.0034	2.304	0.055	0.0806	0.0014	0.693	1215	20	1211	34	0
44	384	349	0.91	28.1	0.005459	9.46	11.763	0.175	0.1457	0.0022	0.0770	0.0019						478	11			
45	176	170	0.97	12.6	0.000473	0.86	11.976	0.227	0.0616	0.0019	0.0828	0.0016						513	10			
46	141	105	0.74	38.2	-	<0.01	3.165	0.054	0.1090	0.0020	0.3161	0.0054	4.775	0.120	0.1096	0.0020	0.682	1771	26	1792	33	1
47	137	78	0.57	43.9	-	<0.01	2.684	0.045	0.1373	0.0021	0.3733	0.0063	7.157	0.162	0.1390	0.0021	0.746	2045	30	2215	26	8
48	503	259	0.52	35.2	0.000513	0.93	12.265	0.167	0.0611	0.0011	0.0808	0.0012						501	7			
49	230	126	0.55	17.1	0.000123	0.22	11.507	0.234	0.0594	0.0016	0.0867	0.0018						536	11			
50	339	75	0.22	27.1	0.001041	1.95	10.749	0.195	0.0595	0.0014	0.0912	0.0017						563	10			
51	628	272	0.43	182.2	0.000263	0.38	2.961	0.038	0.1505	0.0011	0.3365	0.0043	6.826	0.109	0.1471	0.0014	0.794	1870	21	2313	17	24
52	142	77	0.54	10.0	0.000359	0.64	12.223	0.275	0.0628	0.0024	0.0813	0.0019						504	11			
53	98	43	0.44	15.6	-	<0.01	5.403	0.119	0.0741	0.0026	0.1863	0.0041	2.051	0.083	0.0798	0.0027	0.548	1102	22	1193	67	8
54	403	166	0.41	28.5	0.000112	0.20	12.114	0.187	0.0574	0.0013	0.0824	0.0013						510	8			
55	59	53	0.91	6.0	-	<0.01	8.420	0.332	0.0651	0.0048	0.1188	0.0047						723	27			
56	97	84	0.87	7.0	0.001074	2.01	11.981	0.307	0.0587	0.0026	0.0818	0.0021						507	13			
57	315	315	1.00	21.7	0.000532	0.97	12.473	0.223	0.0601	0.0017	0.0794	0.0015						493	9			
58	403	6	0.01	31.4	0.000157	0.28	11.034	0.187	0.0589	0.0016	0.0904	0.0016						558	9			
59	279	136	0.49	20.8	0.001080	1.94	11.489	0.219	0.0719	0.0020	0.0854	0.0017						528	10			
60	332	248	0.75	23.1	0.000683	1.27	12.324	0.229	0.0584	0.0018	0.0801	0.0016						497	9			

Notes :
1. Uncertainties given at the one σ level.
2. f_{206} % denotes the percentage of ^{206}Pb that is common Pb.
3. Correction for common Pb made using the measured ^{204}Pb/^{206}Pb ratio.
4. For % Disc, 0% denotes a concordant analysis.

Table 2 Summary of SHRIMP U-Pb zircon results for sample TH1.

Table 2. Summary of SHRIMP U-Pb zircon results for sample TH1.

Grain	U	Th	Th/U	Pb*	$^{204}Pb/$	f_{206}	Total Ratios $^{238}U/$		$^{207}Pb/$		Radiogenic Ratios $^{206}Pb/$		$^{207}Pb/$		$^{207}Pb/$			Age (Ma) $^{206}Pb/$		$^{207}Pb/$		%
spot	(ppm)	(ppm)		(ppm)	^{206}Pb	%	^{206}Pb	±	^{206}Pb		^{238}U	±	^{235}U		^{206}Pb	±	ρ	^{238}U	±	^{206}Pb	±	Disc
1.1	240	140	0.58	18.3	0.000274	0.49	11.28	0.18	0.0624	0.0014	0.0882	0.0014						545	8			
2.1	1866	1063	0.57	77.2	0.004219	7.18	20.76	0.23	0.1338	0.0010	0.0447	0.0006						282	4			
3.1	597	353	0.59	47.3	-	<0.01	10.85	0.14	0.0603	0.0010	0.0922	0.0012						569	7			
4.1	251	101	0.40	18.0	0.000000	0.00	11.99	0.19	0.0581	0.0014	0.0834	0.0013						516	8			
5.1	663	996	1.50	83.6	0.000747	1.27	6.81	0.09	0.0846	0.0008	0.1449	0.0019	1.479	0.051	0.0740	0.0024	0.373	872	11	1042	65	19
6.1	95	106	1.12	16.8	0.000157	0.26	4.84	0.09	0.0785	0.0016	0.2060	0.0039	2.165	0.064	0.0762	0.0017	0.639	1207	21	1101	45	-9
7.1	78	47	0.60	10.7	-	<0.01	6.27	0.13	0.0709	0.0019	0.1600	0.0034	1.625	0.068	0.0736	0.0026	0.504	957	19	1032	73	8
8.1	111	199	1.80	9.0	-	<0.01	10.54	0.21	0.0600	0.0018	0.0950	0.0019						585	11			
9.1	55	35	0.64	6.8	0.000522	0.89	6.94	0.17	0.0819	0.0028	0.1427	0.0035	1.467	0.074	0.0745	0.0033	0.480	860	19	1056	89	23
10	950	415	0.44	22.2	0.000088	0.12	36.82	1.00	0.1920	0.1051	0.0271	0.0007						173	5			
11	466	0	0.00	183.0	0.000040	0.06	2.19	0.03	0.1603	0.0007	0.4569	0.0054	10.069	0.128	0.1598	0.0008	0.927	2426	24	2454	8	1
12	353	101	0.29	27.0	0.000017	0.03	11.24	0.16	0.0601	0.0027	0.0889	0.0012						549	7			
13	260	60	0.23	14.5	0.000704	1.30	15.39	0.29	0.0606	0.0013	0.0641	0.0013						401	8			
14	788	704	0.89	399.0	-	<0.01	1.70	0.02	0.2336	0.0007	0.5895	0.0066	18.988	0.218	0.2336	0.0007	0.969	2987	27	3077	5	3
15	399	205	0.51	43.7	0.000063	0.11	7.85	0.11	0.0699	0.0009	0.1273	0.0018	1.211	0.029	0.0690	0.0013	0.613	772	11	899	39	16
16	1021	697	0.68	82.6	0.000009	0.02	10.62	0.12	0.0596	0.0006	0.0941	0.0011						580	6			
17	314	43	0.14	22.9	0.000062	0.11	11.76	0.17	0.0597	0.0012	0.0850	0.0013						526	7			
18	494	37	0.07	40.5	0.000149	0.27	10.48	0.15	0.0607	0.0009	0.0952	0.0014						586	8			
19	652	224	0.34	173.9	0.000023	0.04	3.22	0.04	0.1159	0.0006	0.3105	0.0036	4.949	0.063	0.1156	0.0006	0.901	1743	18	1890	10	8
20	160	183	1.14	65.8	0.000105	0.15	2.09	0.03	0.1611	0.0013	0.4800	0.0071	10.804	0.181	0.1632	0.0013	0.883	2527	36	2489	13	-2
21	146	38	0.26	42.1	-	<0.01	2.97	0.05	0.1775	0.0017	0.3363	0.0053	8.251	0.152	0.1779	0.0017	0.848	1869	25	2634	16	41
22	454	456	1.01	34.8	0.000082	0.15	11.18	0.16	0.0614	0.0010	0.0893	0.0013						551	8			
23	165	120	0.73	11.3	0.000271	0.49	12.58	0.26	0.0574	0.0016	0.0791	0.0016						491	10			
24	2380	1272	0.53	108.2	0.004759	8.19	18.90	0.21	0.1379	0.0009	0.0486	0.0006						306	4			
25	308	141	0.46	145.9	-	<0.01	1.82	0.03	0.1970	0.0030	0.5509	0.0077	14.991	0.309	0.1974	0.0030	0.675	2829	32	2805	25	-1
26	152	44	0.29	19.6	0.000209	0.36	6.67	0.11	0.0721	0.0015	0.1493	0.0025	1.423	0.059	0.0691	0.0026	0.411	897	14	902	78	1
27	363	195	0.54	24.0	0.000105	0.19	13.01	0.18	0.0608	0.0011	0.0767	0.0011						476	7			
28	392	229	0.59	105.1	-	<0.01	3.20	0.04	0.1054	0.0008	0.3130	0.0039	4.626	0.067	0.1072	0.0008	0.862	1755	21	1753	13	0
29	301	150	0.50	75.6	-	<0.01	3.42	0.05	0.1029	0.0009	0.2925	0.0039	4.167	0.068	0.1033	0.0010	0.817	1654	20	1684	17	2
30	394	121	0.31	108.4	0.000051	0.08	3.12	0.04	0.1110	0.0008	0.3203	0.0040	4.872	0.073	0.1103	0.0009	0.839	1791	20	1805	15	1
31	340	87	0.26	28.4	-	<0.01	10.30	0.15	0.0628	0.0011	0.0975	0.0014						600	8			
32	568	31	0.06	50.8	0.000122	0.22	9.61	0.12	0.0613	0.0008	0.1039	0.0013						637	8			
33	386	106	0.27	58.0	-	<0.01	5.72	0.07	0.0750	0.0011	0.1749	0.0023	1.828	0.037	0.0758	0.0012	0.635	1039	12	1090	31	5
34	125	99	0.79	56.5	0.000004	0.01	1.91	0.03	0.1795	0.0015	0.5258	0.0086	13.197	0.244	0.1820	0.0016	0.886	2724	40	2672	14	-2
35	304	20	0.07	24.7	-	<0.01	10.57	0.16	0.0612	0.0012	0.0946	0.0014						583	8			
36	547	581	1.06	40.7	-	<0.01	11.55	0.15	0.0608	0.0010	0.0865	0.0011						535	7			
37	1263	1170	0.93	79.4	0.004000	6.90	13.67	0.17	0.1263	0.0010	0.0681	0.0010						425	6			
38	375	153	0.41	103.8	-	<0.01	3.10	0.04	0.1449	0.0010	0.3224	0.0047	6.453	0.105	0.1451	0.0011	0.894	1802	23	2290	12	27
39	214	116	0.54	22.2	0.000184	0.32	8.31	0.16	0.0657	0.0014	0.1199	0.0023						730	13			
40	1387	2028	1.46	55.7	0.003682	6.59	21.38	0.27	0.1111	0.0013	0.0437	0.0006						276	4			
41	200	219	1.10	29.1	0.000115	0.20	5.89	0.10	0.0746	0.0014	0.1695	0.0030	1.706	0.046	0.0730	0.0015	0.653	1010	17	1013	42	0
42	120	48	0.40	9.3	0.000311	0.56	11.08	0.29	0.0617	0.0028	0.0898	0.0024						554	14			
43	210	152	0.72	34.6	0.000373	0.63	5.21	0.09	0.0810	0.0017	0.1906	0.0034	1.990	0.096	0.0757	0.0034	0.369	1125	18	1088	90	-3
44	448	223	0.50	139.0	0.000061	0.09	2.77	0.04	0.1262	0.0010	0.3609	0.0048	6.237	0.099	0.1253	0.0011	0.842	1986	23	2034	15	2
45	191	109	0.57	110.4	-	<0.01	1.49	0.02	0.2650	0.0018	0.6728	0.0107	24.585	0.428	0.2650	0.0018	0.918	3317	41	3277	11	-1
46	2772	1392	0.50	64.5	0.004508	7.75	36.89	0.43	0.1344	0.0013	0.0250	0.0004						159	3			
47	384	168	0.44	158.2	0.000038	0.05	2.08	0.03	0.1869	0.0012	0.4794	0.0063	12.325	0.181	0.1865	0.0012	0.894	2525	27	2711	11	7
48	140	83	0.59	29.4	0.000184	0.30	4.10	0.08	0.0922	0.0018	0.2434	0.0047	3.009	0.166	0.0897	0.0046	0.349	1404	24	1418	99	1
49	41	70	1.73	6.2	0.000745	1.30	5.60	0.18	0.0758	0.0033	0.1816	0.0057	2.245	0.116	0.0897	0.0036	0.613	1076	43	1418	78	24
50	314	133	0.42	23.5	0.000069	0.13	11.48	0.19	0.0567	0.0014	0.0870	0.0014						538	8			
51	150	75	0.50	21.3	-	<0.01	6.04	0.11	0.0932	0.0020	0.1664	0.0032	2.236	0.085	0.0974	0.0032	0.500	992	17	1576	62	59
52	111	58	0.53	51.9	0.000221	0.30	1.83	0.03	0.1877	0.0021	0.5440	0.0102	13.874	0.318	0.1850	0.0024	0.820	2800	43	2698	22	-4
53	121	85	0.70	57.0	0.000045	0.06	1.83	0.03	0.1869	0.0018	0.5476	0.0093	14.069	0.283	0.1864	0.0020	0.847	2815	39	2710	18	-4
54	133	95	0.71	14.7	-	<0.01	7.78	0.16	0.0680	0.0020	0.1291	0.0026						783	15			
55	169	84	0.49	75.4	0.000070	0.10	1.93	0.04	0.1852	0.0017	0.5178	0.0095	13.161	0.277	0.1843	0.0019	0.869	2690	40	2692	17	0
56	292	180	0.62	59.1	0.000057	0.09	4.24	0.07	0.0874	0.0025	0.2359	0.0038	2.882	0.094	0.0886	0.0025	0.496	1366	22	1395	54	2
57	748	317	0.42	62.8	0.000328	0.58	10.23	0.14	0.0660	0.0009	0.0972	0.0014						598	8			
58	168	38	0.22	17.6	0.000165	0.29	8.20	0.18	0.0679	0.0018	0.1215	0.0027						739	15			
59	380	24	0.06	70.5	0.000164	0.28	4.63	0.07	0.0769	0.0011	0.2157	0.0033	2.284	0.048	0.0768	0.0011	0.723	1259	17	1116	29	-13
60	219	120	0.55	96.0	0.000177	0.24	1.96	0.03	0.1933	0.0017	0.5092	0.0077	13.418	0.245	0.1911	0.0019	0.830	2653	33	2752	17	4
61	110	208	1.88	30.0	-	<0.01	3.15	0.06	0.1015	0.0018	0.3211	0.0061	4.917	0.132	0.1111	0.0021	0.710	1795	41	1817	34	1

Notes :
1. Uncertainties given at the one σ level.
2. f_{206} % denotes the percentage of ^{206}Pb that is common Pb.
3. Correction for common Pb made using the measured $^{204}Pb/^{206}Pb$ ratio.
4. For % Disc, 0% denotes a concordant analysis.

Table 3 $^{40}Ar/^{39}Ar$ step-heating analytical results (Girilambone Group).

Table 3 $^{40}Ar/^{39}Ar$ step-heating analytical results (Girilambone Group).

Temp (C)	Cum $\%^{39}Ar$	$^{40}Ar/^{39}Ar$	$^{37}Ar/^{39}Ar$	$^{36}Ar/^{39}Ar$	Vol. ^{39}Ar x10^{-14}mol	%Rad. ^{40}Ar	Ca/K	$^{40}Ar^*/^{39}Ar$	Age (Ma)	± 1s.d. (Ma)
TS6										
Muscovite										
J-value = 0.0086126 ± 0.000022										
550	1.75	**254.80**	**0.0225**	**0.7915**	**0.302**	8.20	0.043	20.93	299.0	29.1
650	4.01	**41.42**	**0.0021**	**0.0225**	**0.388**	83.9	0.004	34.74	472.3	1.8
700	6.42	**39.50**	**0.0001**	**0.0142**	**0.416**	89.3	0.000	35.29	478.8	2.0
750	9.57	**37.53**	**0.0001**	**0.0142**	**0.542**	88.7	0.000	33.30	454.9	3.4
780	12.79	**36.48**	**0.0057**	**0.0136**	**0.555**	88.9	0.011	32.43	444.4	1.8
810	17.13	**35.07**	**0.0001**	**0.0098**	**0.746**	91.6	0.000	32.14	440.8	1.5
840	23.45	**33.87**	**0.0047**	**0.0063**	**1.088**	94.4	0.009	31.97	438.8	2.2
870	33.64	**32.91**	**0.0105**	**0.0041**	**1.755**	96.2	0.020	31.65	434.9	1.5
900	46.92	**32.52**	**0.0006**	**0.0026**	**2.287**	97.5	0.001	31.72	435.7	1.3
950	63.55	**32.43**	**0.0122**	**0.0028**	**2.863**	97.4	0.023	31.59	434.1	1.8
1000	80.59	**32.44**	**0.0014**	**0.0025**	**2.935**	97.6	0.003	31.66	435.0	1.4
1050	96.39	**32.76**	**0.0089**	**0.0036**	**2.720**	96.7	0.017	31.68	435.3	1.6
1100	98.63	**34.43**	**0.0086**	**0.0098**	**0.386**	91.5	0.016	31.50	433.1	2.3
1150	99.49	**37.30**	**0.0254**	**0.0213**	**0.147**	83.1	0.048	30.98	426.6	7.5
1450	100.0 0	**105.68**	**0.2647**	**0.2532**	**0.088**	29.2	0.503	30.84	424.9	23.0
Total		**37.78**	**0.0075**	**0.0204**	**17.220**			31.73	435.8	2.3
TS17										
Muscovite										
J-value = 0.0085982 ± 0.000022										
600	1.91	**107.56**	**0.0664**	**0.2662**	**0.303**	26.8	0.126	28.86	399.9	13.3
700	4.81	**46.15**	**0.0290**	**0.0361**	**0.460**	76.9	0.055	35.46	480.1	4.4
750	8.13	**39.46**	**0.0251**	**0.0190**	**0.528**	85.7	0.048	33.83	460.6	2.9
800	13.99	**35.70**	**0.0063**	**0.0099**	**0.928**	91.7	0.012	32.73	447.4	2.5
825	20.49	**33.95**	**0.0128**	**0.0054**	**1.032**	95.2	0.024	32.34	442.7	2.4
850	30.34	**33.18**	**0.0040**	**0.0030**	**1.562**	97.2	0.008	32.26	441.7	1.3
875	41.41	**34.58**	**0.0061**	**0.0079**	**1.757**	93.2	0.012	32.20	440.9	2.1
900	53.55	**32.54**	**0.0043**	**0.0012**	**1.926**	98.8	0.008	32.17	440.5	1.3
925	65.28	**32.37**	**0.0074**	**0.0015**	**1.861**	98.6	0.014	31.92	437.5	1.4
950	78.02	**32.38**	**0.0016**	**0.0016**	**2.021**	98.4	0.003	31.87	436.9	2.2
1000	92.84	**32.67**	**0.0051**	**0.0013**	**2.351**	98.7	0.010	32.25	441.5	1.6
1050	97.76	**33.10**	**0.0065**	**0.0032**	**0.780**	97.1	0.012	32.14	440.1	3.7
1075	98.60	**36.87**	**0.0008**	**0.0119**	**0.133**	90.4	0.001	33.34	454.7	6.4
1150	99.39	**39.93**	**0.1142**	**0.0107**	**0.127**	92.0	0.217	36.76	495.5	5.2
1450	100.0 0	**91.12**	**0.9828**	**0.1907**	**0.096**	38.2	1.870	34.83	472.6	13.0
Total		**35.63**	**0.0148**	**0.0111**	**15.860**			32.32	442.4	2.3
BDS029B Whole Rock Slate										
J-value = 0.0086087 ± 0.000022										

500	0.65	**154.20**	**0.0346**	**0.4439**	**0.218**	14.9	0.066	22.98	325.6	41.7
550	2.13	**17.59**	**0.0002**	**0.0119**	**0.499**	79.8	0.000	14.04	205.8	2.4
600	3.83	**29.79**	**0.0051**	**0.0071**	**0.575**	92.9	0.010	27.67	385.5	2.5
650	6.69	**33.31**	**0.0038**	**0.0052**	**0.965**	95.3	0.007	31.74	435.8	2.9
700	12.78	**32.79**	**0.0319**	**0.0031**	**2.054**	97.1	0.061	31.84	437.0	1.9
750	22.32	**32.29**	**0.0234**	**0.0021**	**3.215**	98.0	0.044	31.63	434.4	1.8
800	33.03	**31.92**	**0.0125**	**0.0018**	**3.609**	98.2	0.024	31.36	431.1	1.6
850	47.80	**31.99**	**0.0359**	**0.0025**	**4.980**	97.7	0.068	31.24	429.7	1.4
900	65.30	**32.24**	**0.0031**	**0.0015**	**5.899**	98.5	0.006	31.77	436.2	1.7
950	81.28	**32.62**	**0.0235**	**0.0020**	**5.390**	98.1	0.045	32.00	439.0	1.6
1000	92.19	**33.49**	**0.0033**	**0.0019**	**3.679**	98.2	0.006	32.90	449.9	2.2
1050	97.47	**34.83**	**0.0366**	**0.0047**	**1.779**	96.0	0.070	33.43	456.3	2.8
1100	99.18	**37.40**	**0.1638**	**0.0050**	**0.577**	96.0	0.311	35.91	485.9	2.1
1150	99.82	**41.76**	**0.4988**	**0.0138**	**0.215**	90.3	0.948	37.71	507.2	2.6
1450	100.0 0	**135.95**	**2.0036**	**0.3355**	**0.061**	27.2	3.810	36.97	498.5	28.6
Total		**33.43**	**0.0275**	**0.0061**	**33.710**			31.61	434.3	2.1

I) Errors are one sigma uncertainties and exclude uncertainties in the J-value.
ii) Data are corrected for mass spectrometer backgrounds, discrimination and radioactive decay.
iii) Interference corrections: $(^{36}Ar/^{37}Ar)_{Ca}$ = 2.54E-4; $(^{39}Ar/^{37}Ar)_{Ca}$ = 6.51E-4; $(^{40}Ar/^{39}Ar)_{K}$ = 3.0E-2
iv) J-value is based on an age of 98.8 Ma for GA-1550 biotite.

Table 4 $^{40}Ar/^{39}Ar$ step-heating analytical results (sample H26).

Table 4 $^{40}Ar/^{39}Ar$ step-heating analytical results (Sample H26).

Grain No	Step No.	Cum $\%^{39}Ar$	$^{40}Ar/^{39}Ar$	$^{37}Ar/^{39}Ar$	$^{36}Ar/^{39}Ar$	Vol. ^{39}Ar $x10^{-14}mol$	%Rad. ^{40}Ar	Ca/K	$^{40}Ar^*/^{39}Ar$	Age (Ma)	± 1s.d. (Ma)
H26 Muscovite J-value = 0.0085903 ± 0.000022											
1	1	34.66	37.81	0.0177	0.0029	0.6517	97.6	0.0337	36.91	496.8	2.5
	2	70.08	35.20	0.0214	0.0012	2.3030	98.9	0.0407	34.81	471.9	1.5
	3	100.0	36.08	0.0419	0.0004	1.4890	99.6	0.0796	35.91	485.1	1.6
	Total		35.87	0.0277	0.0012	4.4440			35.49	480.0	1.7
2	1	24.89	35.97	0.0168	0.0012	4.0620	98.9	0.0319	35.58	481.2	1.4
	2	55.87	35.90	0.0138	0.0004	0.2705	99.6	0.0262	35.75	483.1	11.7
	3	97.44	36.95	0.0255	0.0019	0.5334	98.4	0.0485	36.35	490.3	3.8
	4	100.0	35.68	0.0292	0.0011	1.0230	99.0	0.0555	35.31	478.0	3.1
	Total		36.00	0.0196	0.0012	1.0230			35.61	481.5	2.4
3	1	24.29	33.95	0.0028	0.0044	0.4247	96.1	0.0054	32.63	445.7	2.3
	2	54.11	35.30	0.0132	0.0009	1.8110	99.2	0.0250	34.99	474.1	2.2
	3	94.19	34.87	0.0152	0.0010	1.1270	99.0	0.0288	34.53	468.6	2.6
	4	100.00	35.68	0.0292	0.0011	1.0230	99.0	0.0555	35.31	478.0	3.1
	Total		35.13	0.0164	0.0013	4.3860			34.72	470.9	2.5
4	1	28.66	35.35	0.0285	0.0056	0.3975	95.2	0.0541	33.66	458.2	2.6
	2	73.50	47.05	0.0003	0.0003	2.2360	99.7	0.0006	46.91	610.8	1.8
	3	100.0	40.92	0.0353	0.0001	3.5410	99.8	0.0671	40.85	542.6	2.0

Total	42.77	0.0222	0.0006	6.1750		42.58	562.4	2.0

I) Errors are one sigma uncertainties and exclude uncertainties in the J-value.
ii) Data are corrected for mass spectrometer backgrounds, discrimination and radioactive decay.
iii) Interference corrections: (36Ar/37Ar)Ca = 2.54E-4; (39Ar/37Ar)Ca = 6.51E-4; (40Ar/39Ar)K = 3.0E-2
iv) J-value is based on an age of 98.8 Ma for GA-1550 biotite.